Measurement Report: Optical Characterization, Seasonality, and Sources of Brown Carbon in Fine Aerosols from Tianjin, North China: Year-round Observations

Zhichao Dong[1], Chandra Mouli Pavuluri[1]*, Peisen Li[1], Zhanjie Xu[1], Junjun Deng[1], Xueyan Zhao[1], Xiaomai Zhao[1], Pingqing Fu[1], Cong-Qiang Liu[1]

[1]Institute of Surface-Earth System Science, School of Earth System Science, Tianjin University, Tianjin 300072, China

Correspondence to: Chandra Mouli Pavuluri (cmpavuluri@tju.edu.cn)

Abstract

To investigate the optical characteristics and sources of brown carbon (BrC) in North China, where the atmospheric aerosol loadings are high and have severe impacts on the Earth's climate system, we collected fine aerosols ($PM_{2.5}$) at an urban site in Tianjin over a 1-year period. We measured the ultraviolet (UV) light absorption and excitation emission matrix (EEM) fluorescence of the water-soluble BrC (WSBrC) and the water-insoluble but methanol-soluble BrC (WI-MSBrC) in the $PM_{2.5}$ using a three-dimensional fluorescence spectrometer. Average light absorption efficiency of both WSBrC ($Abs_{365, WSBrC}$) and WI-MSBrC ($Abs_{365, WI\text{-}MSBrC}$) at 365 nm was found to be highest in winter (10.4±6.76 Mm^{-1} and 10.0±5.13 Mm^{-1}, respectively) and distinct from season to season. Averages of fluorescence index (FI) and biological index (BIX) of WSBrC were lower in summer than in other seasons and opposite to that of humification index (HIX), which implied that the secondary formation and further chemical processing of aerosols were intensive during the summer period than in other seasons. Whereas in winter, the higher HIX together with the higher FI and BIX of WI-MSBrC suggested that the BrC loading was mainly influenced by primary emissions from biomass burning and coal combustion. Based on EEM, the types of fluorophores in WSBrC were divided into humic-like substances (HULIS), including low-oxygenated and high-oxygenated species, and protein like compounds (PLOM), whereas mostly PLOM in the WI-MSBrC. The direct radiation absorption by both WSBrC and WI-MSBrC in the range of 300–400 nm was accounted for ~40% to that (SFE_{Abs}, 4.97±2.71 Wg^{-1} and 7.58±5.75 Wg^{-1}, respectively) in the range, 300–700 nm.

1 Introduction

Brown carbon (BrC) is a part of organic aerosol (OA) and can absorb solar radiation in the near-ultraviolet (UV) to visible (Vis) light, ranging from 300-500 nm (Liu et al., 2013). It has been well recognized that BrC has a significant effect on radiative forcing at both regional and global scales (Feng et al., 2013;Jo et al., 2016;Park et al., 2010). *For example*, the warming effect of water-soluble BrC in the Arctic has been reported to be accounted for ~30% of that exerted by the black carbon (Yue et al., 2022). The BrC not only affects the direct radiative forcing, but also has a potential impact on indirect radiative forcing due to its hydrophilicity, which influences the formation of cloud condensation nuclei (CCN) (Andreae and Gelencs´er, 2006;Laskin et al., 2015b). In addition, BrC is mostly composed of highly conjugated aromatic ring compounds such

40 as a polycyclic aromatic hydrocarbons and high molecular weight substances with a polar
41 functional group that consists of nitrogen and/or oxygen, or humic-like substances (HULIS), which
42 could pose a risk to human health. *For example*, carbon-containing aromatic compounds can cause
43 physical weakness, decreased immunity, arteriosclerosis, etc., which will increase the mortality
44 due to cardiovascular and cerebrovascular diseases and a variety of cancers such as skin cancer,
45 pharyngeal cancer and nasal cancer (Diggs et al., 2011;Peters et al., 2008;Hecobian et al., 2010).

46 BrC can be emitted directly from primary sources such as biomass burning (Hoffer et al.,
47 2006;Brown et al., 2021), fossil fuel combustion (Jo et al., 2016), and non-combustion processes
48 such as bioaerosols (plant debris and fungi) and soil humus (Lin et al., 2014;Rizzo et al.,
49 2013;Rizzo et al., 2011). On the other hand, BrC can also be produced from complex chemical
50 reactions of volatile organic compounds (VOCs) emitted from both anthropogenic and biological
51 origin in gas-pahse as well as by multiphase reactions between the gaseous, particulate and
52 aqueous constituents (Kasthuriarachchi et al., 2020;Li et al., 2020a;Laskin et al., 2015a).

53 In recent times, after establishing the fact that BrC absorb the light, the researchers are paying
54 lot of attention to measure the physical (optical) and chemical characteristics of the BrC and
55 estimate its climatic effects (Yue et al., 2019;Choudhary et al., 2021;Hecobian et al., 2010).
56 However, studies on BrC are still very limited due to difficulties in quantitative measurement of
57 light-absorbing organic components (Corbin et al., 2019;Wang et al., 2022b). In fact, based on the
58 disparity in wavelength dependence between BC and BrC, traditional optical instruments can be
59 used to obtain the BrC absorption value, but the availability of such instruments are limited, which
60 can accurately and directly differentiate the light absorption caused by the BC and BrC. On the
61 other hand, the molecular composition and optical properties of BrC are significantly changed
62 when the BrC is subjected for physical and photo-chemical processing (aging) in the atmosphere.
63 That is why, the indirect approaches have been developed to explore the molecular composition
64 including chromophores and sources of BrC through its light absorption and fluorescence
65 characteristics.

66 UV-Vis spectroscopy and excitation emission matrix (EEM) fluorescence spectroscopy are
67 considered to be common techniques for studying the optical absorption and fluorescence
68 chromophore optical and structural characteristics of complex organic materials, because each
69 chromophore has its own specific excitation-emission peak in the EEM maps (Chen et al.,
70 2016b;Coble, 2007). In recent years, combined spectrophotometric measurement and chemical
71 analysis has been applied to study the BrC in Xi'an, Northwest China (Huang et al., 2018). In fact,
72 EEM fluorescence spectroscopy provides multiple superposed spectral data. By using parallel
73 factor (PARAFAC) analysis of such spectral data, the type of chromophores can be identified and
74 their types are quantified semi-quantitatively based on the range of excitation-emission
75 wavelengths (Cao et al., 2022;Zhan et al., 2022;Murphy et al., 2013). The composition of humic-
76 like and protein-like components have been identified from the analysis of chromophores of
77 dissolved organic substances in aquatic environments (Xie et al., 2020). The fluorescence
78 technique has been widely applied to measure organics in terrestrial and oceanic systems (Murphy
79 et al., 2013;Yu et al., 2015), but has rarely been used in the study of atmospheric aerosols. Now,
80 the application of fluorescence technique has been well established in studying the molecular
81 composition of aerosols as well, the studies on identification of chromophores and thus the
82 molecular composition of BrC in the atmospheric aerosols are still very limited (Wu et al.,
83 2021a;Deng et al., 2022;Li et al., 2022;Cao et al., 2022).

84 Therefore, much attention need to be paid further, particularly on long-term and continuous
85 measurements of the optical characteristics of water-soluble BrC (WSBrC) and their temporal and

spatial variations. Moreover, the investigation of light absorption and fluorescence characteristics of water-insoluble BrC (WIBrC) that can be extracted into a solvent with higher extraction efficiency is necessary to better understand the impact of the BrC on climate change (Corbin et al., 2019). In fact, such studies are very scarce, because the selection of solvents and determination of extraction efficiency are difficult, although different polar chromophores could be extracted by solvent extraction according to the polarity of solvent and methanol has been used as a common solvent (Chen et al., 2016a). Hence, the comprehensive study of the optical properties of WSBrC and WIBrC is highly necessary to better understand the types of chromophores and optical properties of atmospheric aerosols, as well as the processes of oxidation and transformations of chromophores at different locale over the world.

China is one of the most polluted areas in the world, and suffering from the absorption and scattering of solar radiation by atmospheric aerosols that directly affect the energy balance of the Earth's climate system, especially in North China Plain (Wang et al., 2022a). As an important port city in the North China Plain, Tianjin, which has a large population, has received a widespread attention to address the atmospheric environmental issues. Previous studies have shown that BrC in the atmosphere contributes significantly to the light absorption by aerosols (Deng et al., 2022). $PM_{2.5}$ loading in the Tianjin area is extremely high, with greater abundance of organic matter (OM) (Dong et al., 2023a). In such an environment, BrC is likely to become an important light-absorbing component of atmospheric aerosols. However, the studies on physico-chemical characteristics and sources of BrC are very limited in the North China Plain, and to the best of our knowledge, the long-term observations of the optical properties and molecular composition of BrC have not been reported yet over the Tianjin region.

In this study, we measured the optical properties and molecular composition of WSBrC and water-insoluble but methanol-soluble BrC (WI-MSBrC) in fine aerosols ($PM_{2.5}$) collected from Tianjin, North China over a one-year period using the combined UV-Vis absorption and EEM fluorescence spectroscopy technique. We discussed the seasonal variations in optical properties and chromophore composition of WSBrC and WI-MSBrC in the $PM_{2.5}$. We also assessed the possible sources of BrC including the potential photochemical processing of OA (aging) over the Tianjin region, based on the relationships between the BrC and chemical tracers and stable carbon ($\delta^{13}C$) and nitrogen ($\delta^{15}N$) isotope ratios of total carbon (TC) and nitrogen (TN) in the $PM_{2.5}$. Thus, this study provides a comprehensive understanding of the optical characteristics, seasonality, and sources of BrC in the Tianjin region, and warrant the need to develop the prevention and control strategies for the BrC and/or its precursors emissions.

2 Materials and Methods

2.1 Aerosol sampling

Fine aerosol ($PM_{2.5}$) sampling was conducted in Tianjin, a coastal city located at the lower reaches of the Haihe River and Bohai Sea and 150 km away from Beijing in the northern part of China. The sampling took place on the rooftop of a six-storey building at Tianjin University (ND, 39.11°N,117.18°E) in an urban area of Nankai District, Tianjin. A high-volume air sampler (Tisch Environmental, TE-6070DX) at a flow rate of 1.0 m^3 min^{-1} and pre-combusted (6 hours at 450°C) quartz fiber filters (Pallflex 2500QAT-UP) were used for continuously collecting the $PM_{2.5}$ samples for 3 days (~72 hours) each during 5 July 2018 to 4 July 2019 ($n = 121$). Filter blanks were collected twice per season during the sample campaign, following the same sampling procedure placing the filter in hood for 10 mins without turning on the sampler pump.

130   Prior to and after sampling, each filter was dehumidified in a desiccator for 48 hours and
131 determined the PM$_{2.5}$ mass by gravimetric analysis, and then stored in a pre-combusted glass jar
132 with a Teflon-lined cap in the dark at −20°C until analysis.

133   2.2 Measurement of carbonaceous and ionic components

134   Details of the measurements of aerosol organic carbon (OC), element carbon (EC) and water-
135 soluble organic carbon (WSOC) were described by Wang et al. (Wang et al., 2019) and Dong et
136 al. (Dong et al., 2023a). Briefly, concentrations of the OC and EC were measured using an aliquot
137 of filer (1.5. cm^2) and a thermal-optical carbon analyzer (Sunset Laboratory Inc, USA), following
138 the IMPROVE protocol of the protective visual environment. WSOC was measured using an
139 aliquot of filter (one disc of either 14 mm or 22 mm in diameter) extracted into organic-free Milli
140 Q water and total organic carbon (TOC) analyzer (Model OI, 1030W + 1088). Concentrations of
141 K$^+$ and Cl$^-$ were determined using an aliquot of filer (one disc of 22 mm in diameter) extracted
142 into ultrapure water (>18.2MΩ cm) and ion chromatography (ICS-5000 System, China, Dai An)
143 (Dong et al., 2023a). The analytical uncertainty in replicate analyses were within 2 % for OC and
144 5% for EC, WSOC and inorganic ions. Concentrations of all the components were corrected for
145 field blanks.

146   2.3 Measurement of optical properties of brown carbon (BrC)

147   2.3.1 Extraction and concentration of BrC

148   BrC was extracted into 30 ml ultrapure water using a sample filter disc of 22 mm in diameter
149 placed in a glass bottle with screw cap and sealed with Teflon tape under ultrasonication for 30
150 min. The extracts were filtered through a 0.45 μm polytetrafluoron (PTFE) syringe filter to remove
151 the water-insoluble particles and filter debris, and transferred into a clean glass bottle. The extracts
152 were used for the light absorption and fluorescence measurements of WSBrC. While the
153 concentration of WSBrC was considered as the concentration of WSOC.
154   After the extraction of WSBrC, the WI-MSBrC was extracted into 30 ml methanol using the
155 same filter sample left in the same glass bottle with screw cap sealed with Teflon tape under
156 ultrasonication for 30 min. The extracts were filtered using the same 0.45 μm PTFE syringe filter
157 to remove the insoluble particles and filter debris and transferred into another clean glass bottle.
158 The methanol extracts were used for the measurements of optical properties of WI-MSBrC. The
159 concentration of water-insoluble organic carbon (WIOC) was considered as the concentration of
160 WI-MSBrC, which calculated as equation (1), presuming that all the water-insoluble organic
161 contents are dissolved in methanol, although we do not preclude that some of organic species are
162 not soluble in MeOH (Shetty et al., 2019).
163     $WI - MSBrC = OC - WSOC$ (1)
164 2.3.2 Light absorption of BrC
165   A three-dimensional fluorescence spectrometer (Aqualog, Horiba Scientific) was used to
166 record the excitation-emission matrices (EEM) spectra and ultraviolet-visible (UV–Vis)
167 absorption spectra of the solution samples in 1×1 cm quartz cuvettes. The instrument parameters
168 during sample analysis were as follows: The UV-Vis absorption spectra of extracts were recorded
169 in the wavelength range of 240–700 nm. The UV−visible absorption spectra of the solvents were
170 also recorded to subtract their contributions from the extract spectra. The EEM was recorded in
171 the wavelength range of 240–700 nm for excitation and the integration time was 0.1 s with a 1 nm

172   increment. An increment of 8 pixels (5.04 nm) is used as the emission wavelength interval. Prior
173   to sample analysis, the pure solvents of water and methanol (MeOH) were used to obtain the
174   reference signal.

175   Based on the light absorption spectra, the absorption data are converted to the absorption
176   coefficient (Abs: m^{-1}) following equation (2) (Deng et al., 2022;Hecobian et al., 2010):

177    $$Abs_\lambda = (A_\lambda - A_{700}) \times \frac{V_l}{V_a} \times ln(10) \tag{2}$$

178   where A_{700} is the absorption at 700 nm, serving as a reference to account for baseline drift; V_l is
179   the volume of water or MeOH used for extraction; V_a is the volume of sampled air; L is the optical
180   path length (0.01 m). A factor of ln(10) is utilized to convert the log base 10 to a natural logarithm
181   to obtain a base-e absorption coefficient. To compensate for any baseline shift that may occur
182   during analysis, absorption at wavelengths below 700 nm is compared to that of 700 nm where no
183   absorption occurs for ambient aerosol extracts. The average absorption coefficient between 360
184   and 370 nm (Abs_{365}) is used to represent BrC absorption in order to avoid any interferences from
185   non-organic compounds (e.g., nitrate) and to be consistent with the literature values (Huang et al.,
186   2018).
187   Absorption Ångström exponent (AAE, Å) represents the spectral dependence of aerosol light
188   absorption. The spectral dependence of light absorption by chromophores in solution can be
189   described by the following equation (3):

190    $$Abs_\lambda = C \times \lambda^{-AAE} \tag{3}$$

191   where C is a composition-dependent constant; λ is the wavelength (nm). The AAE of the filter
192   extracts is calculated by a formula in the wavelength range of 300–500 nm. The selected range
193   serves two purposes: (1) to prevent any interferences from non-organic compounds at lower
194   wavelengths; (2) to ensure a sufficiented signal-noise ratio for the investigating samples (Huang
195   et al., 2018).

196   The mass absorption efficiency (MAE: $m^2\,g^{-1}$) of the filter extract at wavelength of λ can be
197   characterized as equation (4). The ratio of MAE_{250} to MAE_{365} is denoted as E_2/E_3 to characterize
198   the relative size of molecular weight, which is inversely proportional to the molecular weight.
199   E_2/E_3 is calculated with the method as equation (5).

200    $$MAE_\lambda = Abs_\lambda/M \tag{4}$$
201    $$\frac{E_2}{E_3} = \frac{MAE_{250}}{MAE_{365}} \tag{5}$$

202   where M ($\mu g\,m^{-3}$) is the concentration of WSOC for water extracts and that of WIOC for methanol
203   extracts.

204   The imaginary part (k) of the refractive index (m = n+ik) is derived with the following
205   equation (6) (Liu et al., 2013;Deng et al., 2022):

206    $$k_\lambda = (MAE \times \rho \times \lambda)/4\pi \tag{6}$$

207   where MAE is the mass-absorption cross section of WSBrC or WI-MSBrC ($m^2\,g^{-1}$), ρ is the
208   effective density, λ is the wavelength for the computed MAE including WSBrC and WI-MSBrC.
209   For this study, an effective density of 1.5 g m^{-3} is assumed for WSBrC and WI-MSBrC in the
210   derivation (Liu et al., 2013). MAE values are computed for 365 nm.

211   2.3.2 EEM of BrC and PARAFAC analysis

212   The raw EEMs were first calibrated for the correction of spectrometer factors, which reflect
213   the spectrometer deviation and light source, and then for the inner filter correction, following the
214   procedure described elsewhere (Chen et al., 2019;Gu and Kenny, 2009). Briefly, the inner filter

correction of the EEMs was done based on the UV-Vis light absorbance of the extracts, which was lower than 0.7 in the calibrated wavelength range and is appropriate (Gu and Kenny, 2009). The signal intensity of the EEMs was then normalized to the Raman unit (RU) of water (Lawaetz and Stedmon, 2009). The fluorescence volume (FV, RU-nm^2/m^3) of extracts present in the atmosphere was estimated based on the EEMs at the excitation wavelength ranging from 240 to 700 nm, and then normalized it (i.e., NFV (RU-nm^2-[mg/L]$^{-1}$)) by dividing the FV with the concentration of WSOC and WIOC in the aerosol [mg m^{-3}]).

Various types of chromophores present in the PM$_{2.5}$ samples were classified and identified based on the PARAFAC analysis of the EEMs using the SOLO (Eigenvector Inc.), the data analysis software. PARAFAC analysis was performed for each extraction fluid in each season. Ultimately, three EEM components were determined and assigned to different types of chromophores.

Additionally, fluorescence index (FI) was determined by calculating the ratio of emission intensities at 450 nm and 500 nm after excitation at 370 nm (McKnight et al., 2001). Contributions from local biological sources can be characterized by biological index (BIX), which was calculated using the ratio of emission intensities at 380 and 430 nm following 310 nm excitation (Gao yan and Zhang, 2018). Under the condition of Ex=255 nm, the humification index (HIX) was determined by dividing the area of fluorescence intensity between 435 and 480 nm by that of fluorescence intensity between 300 and 345 nm (Battin, 1998). The calculation formulas (7)– 9) are as follows:

$$FI = \frac{F_{450}}{F_{500}}, \lambda_{Ex} = 370nm \tag{7}$$

$$BIX = \frac{F_{380}}{F_{430}}, \lambda_{Ex} = 310nm \tag{8}$$

$$HIX = \frac{\int 435-480}{\int 300-345}, \lambda_{Ex} = 255nm \tag{9}$$

In formula (6) - (8), λ_{Ex} refers to the excitation wavelength, F_i refers to the fluorescence intensity of emission wavelength at i in the emission spectrum, and $\int i$-j refers to the integrated fluorescence emission intensity in the range of 435–480 nm to 300–345 nm.

2.3.3 Simple forcing efficiency by light absorption of BrC (SFE$_{Abs}$)

It is possible to make a rough estimate of the radiative forcing caused by aerosols using a simple forcing efficiency (SFE, W/g), which reflects the energy added to the Earth's atmospheric system per unit mass of aerosols and can be estimated as described in the literature (Bond and Bergstrom, 2006;Deng et al., 2022), using the following equation (10):

$$\frac{dSFE}{d\lambda} = -\frac{1}{4}\frac{dS(\lambda)}{d\lambda}\tau_{atm}^2(\lambda)(1-F_c)[2(1-a_s)^2\beta(\lambda) \times MSE(\lambda) - 4a_s \times MAE(\lambda)] \tag{10}$$

where dS/dλ is the solar irradiance, τ_{atm} is the atmospheric transmission (0.79), F_c is the cloud fraction (approximately 0.6), a is the surface albedo (average 0.19), β is the backscatter fraction, and MSE and MAE are the mass scattering and absorption efficiency, respectively (Deng et al., 2022).

It is important to note that BrC can affect a strong instantaneous negative forcing through scattering, however it is not possible to evaluate this directly using offline samples because of strong dependency on particle size. That is why, we limited to estimate the radiative effect caused by only the absorption component of the BrC in this study. Therefore, the equation (10) can be simplified to:

$$SFE_{Abs} = \int \frac{dS(\lambda)}{d\lambda} \tau_{atm}^2 (1 - F_c) a_s MAE(\lambda) d\lambda \qquad (11)$$

3 Results and discussion

### 3.1 Characteristics of ultraviolet light absorption of WSBrC and WI-MSBrC

3.1.1 Absorption coefficient (Abs)

Annual and seasonal averages of various optical properties of WSBrC and WI-MSBrC in PM$_{2.5}$ measured in this study are summarized in Table 1. Their ranges and median values are provided in supplement Table S1. Temporal variations in absorption coefficient of WSBrC at 365 nm (Abs$_{365(WSBrC)}$) and that of WI-MSBrC (Abs$_{365(WI-MSBrC)}$) together with the concentrations of WSOC and WIOC are depicted in Fig. 1. Because the light absorption at the wavelength of 365 nm would not be interfered by inorganic substances (Hecobian et al., 2010), the Abs at 365 nm was selected for the analysis in this study. Abs$_{365(WSBrC)}$) ranged from 0.49 Mm^{-1} to 36.7 Mm^{-1} with an average of 4.74 Mm^{-1} during the campaign. While the Abs$_{365(WI-MSBrC)}$ ranged from 0.32-25.0 Mm^{-1} (avg. 3.87 Mm^{-1}) during the campaign. Temporal trends of Abs$_{365(WSBrC)}$ were found to be similar with those of Abs$_{365(WI-MSBrC)}$, with the lowest levels in summer followed by a gradual increase toward autumn and peak in winter and then a gradual decrease toward spring during the campaign (Fig. 1). Furthermore, those trends were highly comparable to those of the concentrations of both WSOC and WIOC in PM$_{2.5}$ (Fig. 1). The correlations between Abs$_{365(WSBrC)}$ and WSOC and Abs$_{365(WI-MSBrC)}$ and WIOC were found to be strong (R = 0.93 and 0.96, respectively) during the campaign. These results indicate that both WSBrC and WI-MSBrC might have been derived from the same or similar sources including the secondary processes, and their light absorbance should have been significantly dependent on their abundances that varied from season to season (Fig. 1; Table 1).

Averages of both Abs$_{365(WSBrC)}$ and Abs$_{365(WI-MSBrC)}$ were higher in winter followed by autumn and spring and the lowest in summer (Table 1). The high Abs$_{365}$ of BrC in winter might have been mainly driven by the existence of large amounts of organic aerosols, whereas the lowest Abs$_{365}$ in summer might be due to enhanced decomposition of BrC constituents by photobleaching under high solar radiation and oxidants loading in the atmosphere, which is unlikely in the wintertime. The seasonal variations of both Abs$_{365(WSBrC)}$ and Abs$_{365(WI-MSBrC)}$ in Tianjin were similar to those of the Abs$_{365}$ of WSBrC reported in the southeastern United States, but their values (Table 1) were much higher than that (0.3–3.0 Mm^{-1} in 2007) in the southeastern United States (Hecobian et al., 2010) as well as that in Atlanta and Los Angeles (0.88 ± 0.71 and 0.61 ± 0.38 Mm^{-1}, respectively) in summer 2010 (Zhang et al., 2011). Biomass burning was considered to be the dominant source of BrC at the southeastern United States in colder period, whereas both primary emissions from fossil fuel combustion and secondary formation were significant in summertime (Hecobian et al., 2010). While the SOA formed from fresh anthropogenic and biogenic VOCs were considered to be major at Atlanta and Los Angeles, respectively (Zhang et al., 2011).

It has been reported that the solid fules (i.e., biomass or coal) combustion is dominant and the Abs$_{370}$ of BrC is reported to be high (21.8 Mm^{-1}) in North China cities (Zhang et al., 2021). It has also been reported that the Abs$_{370}$ of BrC produced by residential wood burning is much higher, reaching up to 37.1 ± 74.6 Mm^{-1} in Athens in winter (Liakakou et al., 2020). The maximum Abs$_{365(WSBrC)}$ and Abs$_{365(WI-MSBrC)}$ in Tianjin aerosols were 36.7 and 25.0 Mm^{-1}, respectively, which are comparable to those of wood combustion samples. However, their ranges found to be

large during the campaign (Fig. 1; Table S1), suggesting that in addition to biomass burning, the other emission sources and meteorological conditions in different seasons should have been played an important role in controlling the WSBrC and WI-MSBrC loadings and their optical characteristics in the Tianjin atmosphere. Furthermore, the $Abs_{365(WSBrC)}$ observed in this study (Table 1) is slightly lower compared to that reported in Tianjin during winter 2016 (14.1 ± 8.5 Mm^{-1}) and summer 2017 ($2.1 \pm 1.0 Mm^{-1}$) (Deng et al., 2022) as well as that reported in Beijing and Xi'an, which are considered to be highly polluted cities in northern China (Huang et al., 2020;Li et al., 2020b). However, the $Abs_{365(WSBrC)}$ and $Abs_{365(WI-MSBrC)}$ found in winter in this study were higher than that reported at different locations in southern China; Nanjing ($Abs_{365(WSBrC)} = 4.84 Mm^{-1}$, $Abs_{365(MSBrC)} = 7.75 Mm^{-1}$) (Xie et al., 2020), Guangzhou ($Abs_{365(WSBrC)} = 8.8 Mm^{-1}$) (Li et al., 2018), and Lhasa ($Abs_{365(WSBrC)} = 1.04 Mm^{-1}$, $Abs_{365(MSBrC)} = 1.47 Mm^{-1}$) (Zhu et al., 2018), where the fossil fuel combustion is considered as the dominant source. Such higher Abs_{365}, particularly in winter, indicates that BrC in $PM_{2.5}$ in Tianjin might have been derived from mixed sources such as biomass burning and fossil fuel (coal) combustion and has a significant effect on light absorption and thus on climate system over the region.
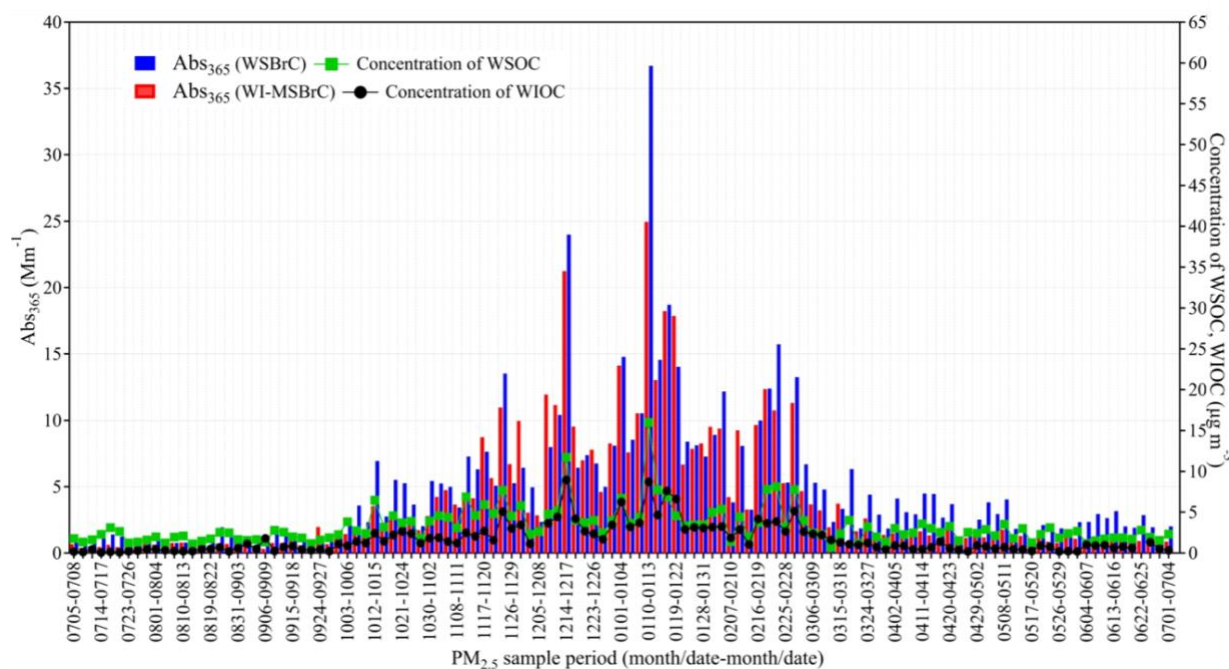

Figure 1. Temporal variations of the light absorption coefficient of water-soluble brown carbon (BrC) at 365 nm ($Abs_{365(WSBrC)}$) and water-insoluble but methanol-soluble BrC ($Abs_{365(WI-MSBrC)}$) and the mass concentrations of WSOC and WIOC in $PM_{2.5}$ in Tianjin, North China during 2018 and 2019. WSOC and WIOC mass concentrations data was obtained from (Dong et al., 2023b).

Figure 2 shows the seasonal average absorption spectra of WSBrC and WI-MSBrC at wavelengths of 240−700 nm, which shows a common feature that the absorption of shorter wavelengths increases sharply and significantly. Such feature is different from the absorption characteristics of BC, whose AAE is close to 1 and weakly dependent on the wavelength. Another evident feature of BrC absorption spectra shown in Figure 2 is that the Abs of WI-MSBrC was always greater than that of WSBrC across the shorter wavelengths in winter and in the range of 260~300 nm in other seasons, which is consistent with the pattern reported in the literature (Huang

8

et al., 2020;Li et al., 2020b). In addition, the Abs of WI-MSBrC peaked at 280 nm, but not that of WSBrC (Fig. 2). Such patterns can be attributed to the difference in types and amounts of chromophores soluble in water and methanol (e.g., PAHs are soluble in methanol, but not in water). It is noteworthy that, $\pi-\pi*$ electron transitions in the double bonds of aromatic compounds are the primary cause of light absorption in the wavelength range of 250−300 nm. It has been reported in another study that nitroaromatics have contributed 60% to the total absorbance in the 300-400 nm range (Hems et al., 2021). The electron transitions in phenolic arenes, aniline derivatives, polyenes and polycyclic aromatic hydrocarbons with two or more rings are responsible for the absorbance in the bands between 270 and 280 nm (Baduel et al., 2009). Therefore, the differences observed in the Abs of WSBrC and WI-MSBrC imply that the aromatic and/or unsaturated aliphatic organic compounds are abundant in $PM_{2.5}$ in Tianjin, which are more soluble in MeOH than in water.

High correlations (R = 0.73-0.97) were found between Abs_{365} of both WSBrC and WI-MSBrC and WSOC and WIOC in each season, except in summer (R = 0.20-0.62) (Figure S1). As noted earlier, such linearity of Abs_{365} with WSOC and WIOC indicate that WSBrC and WI-MSBrC might have been derived from similar sources including the secondary processes over the Tianjin region, except in summer, because the light absorption efficiency of organic compounds of different origin are different and significantly depend on their secondary processes in the atmosphere (Zhong and Jang, 2011). In fact, the Abs depends on the amount of BrC availability, but not of total OC content. In summer, the BrC loading might be less due to either photobleaching under the enhanced aging and/or less availability of N and/or S species to produce N- and S-containing organics (BrC) in the atmosphere over the Tianjin region.
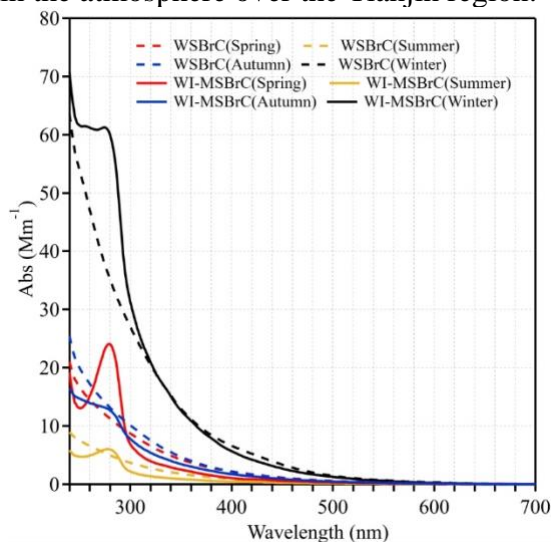
Figure 2. Seasonal averages of absorption spectra in the wavelength range of 240–700 nm of WSBrC and WI-MSBrC in $PM_{2.5}$ from Tianjin, North China.

The moderate to high positive correlations (R = 0.51-0.92) found between both $Abs_{365(WSBrC)}$ and $Abs_{365(WI\text{-}MSBrC)}$ and K^+ and Cl^- in all seasons, except between Abs_{365} WSBrC and Cl^- in summer (R = 0.29) (Fig. S2), suggest that biomass burning and coal combustion were major sources (Dong et al., 2023a) of BrC in the Tianjin region. The poor correlation between Abs_{365} and K^+ was driven by two outliers obtained in K^+ data that might have occurred due to unknown biomass burning events at local scale. In addition, the correlation between $Abs_{365(WSBrC)}$ and K^+ was relatively stronger than that between the $Abs_{365(WI\text{-}MSBrC)}$ and K^+, except in summer (Fig. S2), which support

356 that the chromophores, like nitrophenols, derived from biomass burning are potentially more
357 water-soluble (Li et al., 2020b). While the correlation between $Abs_{365(WI-MSBrC)}$ and Cl^- was
358 relatively stronger than that between $Abs_{365(WSBrC)}$ and Cl^- in spring and summer and comparable
359 in autumn, which suggest that the chromophores derived from fossil fuel (e.g., coal) combustion
360 are slightly more soluble in MeOH compared to that in water, and were abundant in the spring and
361 summer time in Tianjin.
362

Table 1. Mass concentrations of WSOC, WIOC and absorbance efficiency of WSBrC and WI-MSBrC (Avg. ± SD) in $PM_{2.5}$ from Tianjin, North China.

		Annual	Summer	Autumn	Winter	Spring
Concentrations						
WSOC ($\mu g\,m^{-3}$)		3.25 ± 2.18	1.88±0.53	3.45±1.71	5.06±2.99	2.48±0.82
WIOC ($\mu g\,m^{-3}$)		1.68 ± 1.77	0.43±0.32	1.55±1.04	3.74±2.09	0.88 ± 0.63
Optical parameters						
WSBrC	$Abs_{365}(Mm^{-1})$	4.74±5.10	1.47±0.77	3.71±2.83	10.4±6.76	3.45±2.29
	$MAE_{365}(m^2\,g^{-1})$	1.28±0.66	0.80±0.44	0.96±0.33	2.04±0.46	1.31±0.55
	AAE (300–500 nm)	5.66±0.82	5.17±0.83	6.21±0.65	5.88±0.58	5.42±0.74
	E_2/E_3	5.36±0.91	5.64±1.21	5.78±0.83	5.19±0.44	4.83±0.64
	FI	1.38±0.09	1.31±0.07	1.47±0.07	1.37±0.02	1.37±0.09
	BIX	1.05±0.13	0.91±0.06	1.06±0.08	1.20±0.08	1.01±0.11
	HIX	2.87±0.53	3.12±0.44	3.11±0.51	2.47±0.43	2.76±0.47
	k_{365}	0.056±0.029	0.035±0.020	0.042±0.015	0.089±0.021	0.057±0.024
	$SFE_{Abs300-400}$ ($W\,g^{-1}$)	1.95±1.02	1.21±0.67	1.99±0.84	3.12±0.71	1.46±0.52
	$SFE_{Abs300-700}$ ($W\,g^{-1}$)	4.97±2.71	3.68±2.58	5.12±2.17	7.60±2.17	3.39±1.42
WI-MSBrC	$Abs_{365}(Mm^{-1})$	3.87±4.69	0.74±0.25	2.83±2.51	10.0±5.13	1.99±1.95
	$MAE_{365}(m^2\,g^{-1})$	2.36±1.26	2.50±1.78	1.86±1.02	2.69±0.36	2.41±1.28
	AAE (300–500 nm)	6.06±1.23	5.49±1.26	6.11±1.86	6.30±0.27	6.27±0.90
	E_2/E_3	6.60±2.04	6.79±1.32	5.77±1.35	6.20±0.44	7.60±3.25
	FI	1.60±0.13	1.58±0.12	1.57±0.06	1.73±0.11	1.51±0.11
	BIX	1.26±0.21	1.32±0.18	1.05±0.14	1.43±0.09	1.23±0.18
	HIX	0.81±0.60	0.25±0.08	1.23±0.61	1.33±0.30	0.42±0.28
	k_{365}	0.104±0.057	0.109±0.079	0.081±0.045	0.117±0.016	0.105±0.057
	$SFE_{Abs300-400}$ ($W\,g^{-1}$)	2.98±1.70	1.21±0.67	2.98±1.52	4.13±0.57	3.61±1.91
	$SFE_{Abs300-700}$ ($W\,g^{-1}$)	7.58±5.75	3.68±2.58	8.69±9.23	9.36±4.51	8.70±5.03

3.1.2 Absorption Ångström exponent (AAE)

The magnitude of the AAE can reflect the sources and atmospheric chemical processes of BrC (Lack et al., 2013), because the AAE of the BrC emitted from fossil fuel combustion found to be ~1 and that from biomass burning range from 1 to 3 and that derived by secondary formation/transformations vary from 3-7 (Yan et al., 2018). It has also been reported that the AAE of light-absorbing organic species (i.e., BrC) is much larger than that of soot (BC). The AAE was found to be between 2 and 4 for the particles containing both soot and BrC. Furthermore, AAE value of particulate matter is closely related to its chemical composition, mixing state, particle size and other factors. *For example*, Sun et al. (2007) reported that the average AAE of coal briquettes is 2.55 ± 0.44 whereas that of the coal chunks is 1.30 ± 0.32 (Sun et al., 2017). However, it is important to note that unlike the direct measurement of AAE of the particulate matter, the light absorption characteristics of organic components extracted into solvent are not affected by particle size and mixing state of aerosols, but depend on their composition. The AAE of humic-like substances (HULIS) isolated from biomass burning aerosols by water extraction followed by the separation with exchange column was reported to be 6-7 (Hoffer et al., 2006).

The AAE of WSBrC in PM$_{2.5}$ from Tianjin ranged from 3.85 to 7.99 with an average of 5.66 during the campaign. The seasonal averages were highly comparable with each other, except a little higher level in autumn (Table 1). The average AAE of WSBrC in Tianjin (Table 1) is comparable to that (5.1 ± 2.0) reported from New Delhi, India and Beijing (5.3 ± 0.4 in winter and 5.8 ± 0.5 in summer) and the outflow region (6.4 ± 0.6) of northern China (Lesworth et al., 2010). The AAE of WSBrC in Tianjin was also similar to that (range, 6–8) reported in the particulate matter at the southeastern United States (Hecobian et al., 2010) and downtown Atlanta (Liu et al., 2013), where both biogenic and fossil fuel combustion emissions and secondary processes are considered as significant sources. Such higher levels and comparisons of the AAE of WSBrC imply that the OA in Tianjin should have been derived from mixed sources and substantially polar, because the AAE of BrC is increased with its increasing polarity (Chen et al., 2016a).

However, the AAE of WI-MSBrC in Tianjin ranged from 2.08–12.9 (avg. 6.06) and was comparable with that of WSBrC. Furthermore, the averages of AAE of WI-MSBrC in each season were comparable with the other, except a relatively lower level in summer, and also with those of the AAE of WSBrC (Table 1). Generally, the water insoluble portion is expected to have a stronger absorption and weaker wavelength dependence (Saleh, 2020). It has also been reported that the AAE values of the water extract are greater than those of the acetone and methanol extracts (Shetty et al., 2019), and interpreted that the extraction efficiency of polycyclic aromatic hydrocarbons from methanol or other organic solvents is higher than that from water, leading to a higher absorption at longer wavelengths in the methanol extract and therefore a lower AAE value. However, it has also been found that the value of AAE$_{300-600}$ of water extract of biomass burning samples is lower than that extracted into acetonitrile (Lin et al., 2017), indicating that the origin of the BrC is also play an important role. Such comparability between the AAE of WSBrC and WI-MSBrC is consistent with the pattern reported in urban Beijing during winter and Xi'an, China (Li et al., 2020b), where the emissions from fossil fuel combustion are dominant. These results and their comparisons again support that the BrC might have significantly derived from mixed sources (biomass burning and fossil fuel combustion).

407   3.1.3 Mass absorption efficiency (MAE) and imaginary refractive index (k)

408   MAE provides the light absorbing ability of BrC. The MAE_{365} of WSBrC ($MAE_{365(WSBrC)}$)
409 ranged from 0.38 $m^2 g^{-1}$ to 3.41 (avg. 1.28 $m^2 g^{-1}$) and lower by 2 times than that (range, 0.18-7.05
410 $m^2 g^{-1}$; avg. 2.36 $m^2 g^{-1}$) of WI-MSBrC ($MAE_{365(WI-MSBrC)}$) during the campaign in Tianjin.
411 Although the seasonal averages of both $MAE_{365(WSBrC)}$ and $MAE_{365(WI-MSBrC)}$ were higher in winter
412 (1.28 and 2.36 $m^2 g^{-1}$, respectively), the former showed the second most value in spring followed
413 by autumn and the lowest value in summer, whereas the latter showed second most value in
414 summer followed by spring and the lowest value in autumn (Table 1). Furthermore, the average
415 $MAE_{365(WSBrC)}$ in winter was 2.5 times higher than that in summer, which is similar to that (1.8
416 times) reported earlier in Tianjin (Deng et al., 2022), whereas the difference between the averages
417 of $MAE_{365(WI-MSBrC}$ in winter to autumn is 1.4 times only. The seasonal variations of $MAE_{365(WSBrC)}$
418 and $MAE_{365(WI-MSBrC)}$ found in this study are similar to those reported in Xi'an (Li et al., 2020b).
419   The imaginary refractive index (k) is another important parameter that represent the light
420 absorbing ability of carbon and applied in climate model to assess the direct radiative forcing of
421 aerosols. The k of WSBrC ($k_{365(WSBrC)}$) and WI-MSBrC ($k_{365(WI-MSBrC)}$) in Tianjin ranged from
422 0.017 to 0.149 and 0.008-0.307, respectively, in Tianjin. Interestingly, the average $k_{365(WI-MSBrC)}$
423 was 1.9 times to that of $k_{365(WSBrC)}$ during the campaign (Table 1) and their seasonal patterns were
424 also exactly similar to those of the $MAE_{365(WSBrC)}$ and $MAE_{365(WI-MSBrC)}$ (Table 1).
425   Both these MAE_{365} and k_{365} results indicate that most of light-absorbing chromophores are
426 insoluble in water but soluble in MeOH, and their abundances are significantly varied from season
427 to season. Such large seasonal differences indicate that the BrC sources and formation and/or
428 transformation including the degradation (photobleaching) processes might be different in each
429 season. The higher levels of MAE_{365} and k_{365} in winter suggest that the contributions of OA from
430 coal combustion and biomass burning emissions were significantly higher than that in other
431 seasons due to increased residential heating activities. The lower $MAE_{365(WSBrC)}$ and $k_{365(WSBrC)}$ and
432 the second most values of $MAE_{365(WI-MSBrC)}$ and $k_{365(WI-MSBrC)}$ in summer imply that the
433 contributions of OA from fossil fuel combustion emissions might be dominant and the subsequent
434 photobleaching of WSBrC might be significant under high solar radiation in the summertime.
435   The ratio of MAE_{250} to MAE_{365}, which is inversely correlate with the molecular size and
436 aromaticity (Chen et al., 2016c), of WSBrC ($E_2/E_{3(WSBrC)}$) and WI-MSBrC ($E_2/E_{3(WI-MSBrC)}$) in
437 Tianjin ranged from 3.30 to 6.25 with an average of 4.83 and 4.50-24.1 (avg. 7.61), respectively,
438 during the campaign. Interestingly, the averages of $E_2/E_{3(WSBrC)}$ were comparable in summer and
439 autumn and higher than that in winter and spring (Table 1). Whereas the average $E_2/E_{3(WI-MSBrC)}$
440 was higher in spring followed by summer and winter and the lowest in autumn, and higher than
441 the $E_2/E_{3(WSBrC)}$ in each season, except in autumn. Both $E_2/E_{3(WSBrC)}$ and $E_2/E_{3(WI-MSBrC)}$ in each
442 season were comparable or relatively higher than the E_2/E_3 of HULIS (4.7 ± 0.27 for herbaceous
443 plants, 3.6 ± 0.18 for shrubs, 4.2 ± 0.77 for evergreen trees, 4.0 ± 0.82 for deciduous trees, 5.8 ±
444 0.5 for rice straw, 4.5 ± 0.2 for corn straw and 4.4 ± 0.3 for pine branches) emitted from biomass
445 burning (Tang et al., 2020) and lower than that (14.7 ± 0.7) of HULIS emitted from coal
446 combustion (Fan et al., 2016). Thus, the $E_2/E_{3(WSBrC)}$ and $E_2/E_{3(WI-MSBrC)}$ and their comparisons
447 with source signatures indicate that both WSBrC and WI-MSBrC in $PM_{2.5}$ over the Tianjin region
448 should have been mainly derived from biomass burning followed by coal combustion and consist
449 of high aromaticity and large in molecular size.

450   3.2 Direct radiative forcing of WSBrC and WI-MSBrC

451   Radiative forcing efficiency of WSBrC and WI-MSBrC were calculated by integrating the
452 wavelength dependent SFE_{Abs} from 300 nm to 700 nm ($SFE_{Abs300-700(WSBrC)}$ and $SFE_{Abs300-700(WI-MSBrC)}$
453 $_{MSBrC)}$, respectively) in this study. The $SFE_{Abs300-400}$ was also integrated to estimate the radiative
454 forcing efficiency of WSBrC ($SFE_{Abs300-400(WSBrC)}$) and WI-MSBrC ($SFE_{Abs300-400(WI-MSBrC)}$),
455 because the BrC strongly absorbs light in the UV-Vis range. The temporal variations of SFE_{Abs} of
456 WSBrC and WI-MSBrC in both the wavelength ranges are shown in Fig. 3. $SFE_{Abs300-700(WSBrC)}$
457 and $SFE_{Abs300-400(WSBrC)}$ ranged from 0.98 Wg^{-1} to 13.1 Wg^{-1} with an average of 4.97 Wg^{-1} and
458 0.60-5.13 Wg^{-1} (avg. 1.95 Wg^{-1}), respectively. Whereas the $SFE_{Abs300-700(WI-MSBrC)}$ and $SFE_{Abs300-}$
459 $_{400(WI-MSBrC)}$ were 0.92-51.3 Wg^{-1} (7.58 Wg^{-1}) and 0.64-8.84 Wg^{-1} (2.98 Wg^{-1}), respectively, and
460 were higher by 1.5 times than that of the $SFE_{Abs300-700(WSBrC)}$ and $SFE_{Abs300-400(WSBrC)}$ (Table 1).
461 Further both integrated average $SFE_{Abs300-700(WSBrC)}$ and $SFE_{Abs300-700(WI-MSBrC)}$ were higher by 2.5
462 times to that of the $SFE_{Abs300-400(WSBrC)}$ and $SFE_{Abs300-400(WI-MSBrC)}$ (Table 1). Temporal variations
463 of both the $SFE_{Abs300-400(WSBrC)}$ and $SFE_{Abs300-700(WSBrC)}$ were found to be quite similar with a clear
464 seasonal pattern with the lowest levels in summer followed by a gradual increase toward autumn
465 to peak in winter and then a gradual decrease toward spring to the lowest levels in summer, except
466 a sharp rise in early summer 2019 (Fig. 3). Whereas the $SFE_{Abs300-400(WI-MSBrC)}$ and $SFE_{Abs300-700(WI-}$
467 $_{MSBrC)}$ showed exactly the similar temporal pattern with each other, but different from that of the
468 $SFE_{Abs300-400(WSBrC)}$ and $SFE_{Abs300-700(WSBrC)}$ (Fig.3). The levels of $SFE_{Abs300-400(WI-MSBrC)}$ and
469 $SFE_{Abs300-700(WI-MSBrC)}$ found to be relatively stable throughout each season, except in spring, with
470 higher level in spring followed by winter and lower levels in summer (Fig. 3). In consistent with
471 these seasonal patterns, the seasonal variations of $k_{365(WSBrC)}$ and $k_{365(WI-MSBrC)}$, a vital parameter
472 that reflect the light absorbing ability and used in the estimation of radiative forcing by climatic
473 model (Shamjad et al., 2016), were also showed the similar pattern (Fig. S3).
474   The SFE_{Abs} of both WSBrC and WI-MSBrC in both the spectral ranges were higher in winter
475 (Table 1). However, $SFE_{Abs300-400(WSBrC)}$ and $SFE_{Abs300-700(WSBrC)}$ showed the second higher values
476 in autumn and the lowest and comparable values in summer and spring (Table 1). Whereas
477 $SFE_{Abs300-400(WI-MSBrC)}$ and $SFE_{Abs300-700(WI-MSBrC)}$ showed the second higher and comparable values
478 in spring and autumn and the lowest values in summer (Table 1). It is noteworthy that the
479 $SFE_{Abs300-400(WSBrC)}$, $SFE_{Abs300-700(WSBrC)}$, $SFE_{Abs300-400(WI-MSBrC)}$ and $SFE_{Abs300-700(WSBrC)}$ were
480 higher by 61%, 52%, 71% and 61%, respectively, in winter than those in summer, indicating that
481 BrC abundance and strong light absorption capacity of BrC in winter led to a significant increase
482 in direct radiative forcing by the BrC. Furthermore, $SFE_{Abs300-400}$ accounted for 40% of $SFE_{Abs300-}$
483 $_{700}$ in both the fractions of BrC during the whole campaign period and their seasonal averages
484 varied between 33-44%, which are similar to that reported in Tianjin by Deng et al. (2022),
485 indicating the light absorption by BrC in UV-Vis range play a significant role in the total BrC
486 radiative forcing.
487   Furthermore, it is important to note that it has been reported that direct radiative effect of
488 WSBrC is 12.5%% and 13.5% relative to black carbon (BC) radiative forcing in the 280-4000 nm
489 range in summer and winter, respectively, in Tianjin (Deng et al., 2022). In fact, as noted above,
490 the annual average $SFE_{Abs300-700(WI-MSBrC)}$ is higher by 1.5 times to that of $SFE_{Abs300-700(WSBrC)}$
491 (Table 1) in Tianjin. Therefore, the direct radiative effect of total ($\sum$WSBrC+WI-MSBrC) BrC
492 relative to BC would become ~32.5% in Tianjin, revealing that the BrC play a greater role in light
493 absorbing aerosols in the shorter wavelength region in comparison to the entire spectrum.
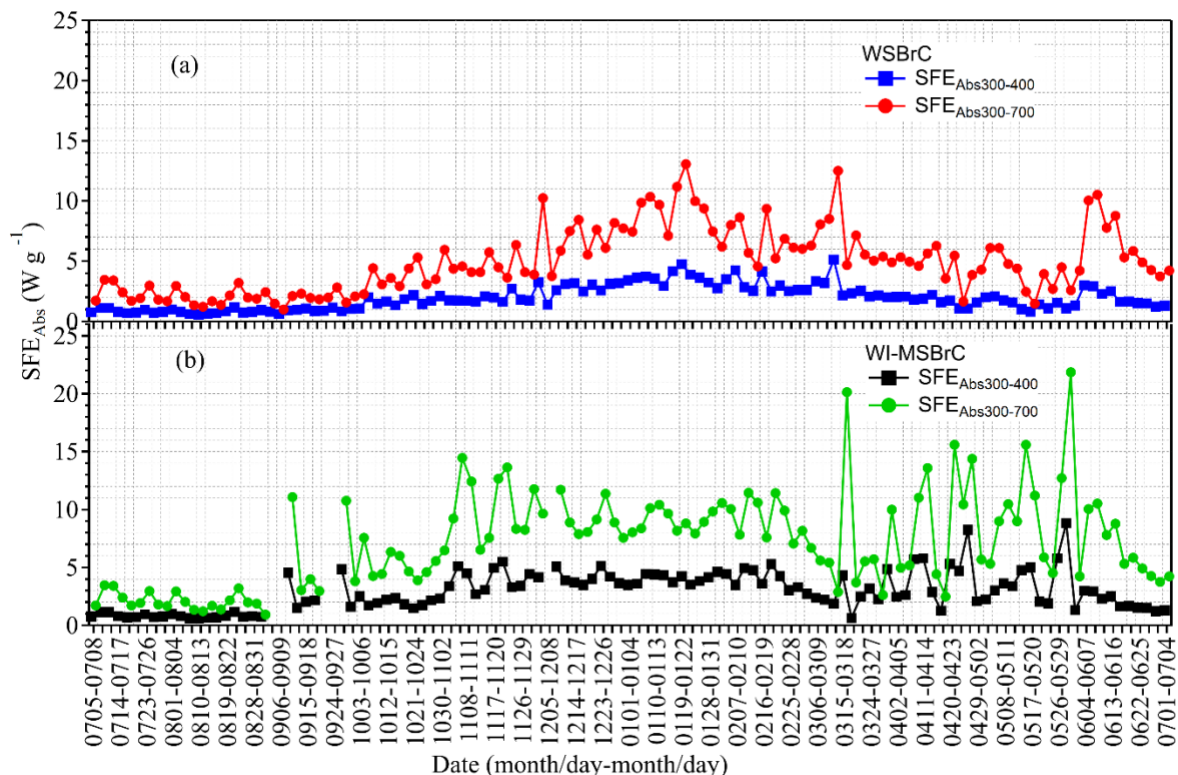
Figure 3. Temporal variations in SFE_{Abs} of WSBrC and WI-MSBrC from 300–400nm and 300–700nm in $PM_{2.5}$ from Tianjin.

3.3 Fluorescence characteristics of WSBrC and WI-MSBrC

3.3.1 Fluorescence indices

Annual and seasonal averages of the fluorescence indices: FI, BIX and HIX, of WSBrC (FI_{WSBrC}, BIX_{WSBrC} and HIX_{WSBrC}, respectively) and WI-MSBrC ($FI_{WI-MSBrC}$, $BIX_{WI-MSBrC}$ and $HIX_{WI-MSBrC}$, respectively) in $PM_{2.5}$ at Tianjin are presented in Table 1. Their ranges and median values are provided in Table S1, and temporal variations are depicted in Fig. 3. Fluorescence indices are developed as indicators for the type and source of the fluorescent organic matter (OM) in aquatic and soil systems and has been successfully applied to assess the sources and aging processes of OA in the atmosphere in recent times (Dong et al., 2023b;Lee et al., 2013;Wu et al., 2021b). FI and BIX provide the insights in exploring the source and aging of OA and received much attention in recent times (Xie et al., 2020;Gao yan and Zhang, 2018;Qin et al., 2018;Deng et al., 2022). They have been considered as indicators to assess the relative contributions of terrestrial, biological and microbially derived OM to OA. The FI values of OM lower than 1.4 indicate its terrestrial origin and the values of 1.9 or higher indicate the microbial origin, and shows an inverse relationship with aromaticity of the OM (Gao yan and Zhang, 2018;Birdwell and Engel, 2010). The BIX values of 0.8 and 1.0 correspond to the freshly derived OM of biological or microbial origin and those of ~0.6 imply the little contribution of the biological OM (Birdwell and Engel, 2010;Dong et al., 2023b). HIX reflect the degree of humification of OA, and has been considered as a proxy for aromaticity of OM and the HIX value is increased with the increasing

15

aromaticity and polycondensation degree (Deng et al., 2022;McKnight et al., 2001;Birdwell and Engel, 2010). The HIX values of >5 reflect the fresh OM derived from biomass and animal manure (Birdwell and Engel, 2010).

FI_{WSBrC} and $FI_{WI-MSBrC}$ were ranged from 1.13 to 1.63 with an average of 1.38 and 1.29-2.24 (avg. 1.60), respectively, during the campaign in Tianjin. While BIX_{WSBrC} and $BIX_{WI-MSBrC}$ were 0.79-1.39 (1.05) and 0.83-1.76 (1.26), respectively, during the campaign. Both FI and BIX of WSBrC and WI-MSBrC followed a temporal pattern, but the temporal pattern of FI_{WSBrC} was exactly opposite to that of the $FI_{WI-MSBrC}$ (Fig. 4a). The FI_{WSBrC} values were slightly decreased from summer to autumn followed by a gradual increase to mid-winter and then a gradual decrease to summer through spring (Fig. 4a). While the temporal variations of BIX_{WSBrC} showed a gradual decrease from summer to autumn followed by a gradual increase to winter and remained relatively stable during the wintertime followed by a gradual decrease to to summer through spring (Fig. 4b). The temporal variations of $BIX_{WI-MSBrC}$ were also found to be opposite to those of the BIX_{WSBrC}, except in winter, in which the $BIX_{WI-MSBrC}$ values were higher compared to those in other seasons (Fig. 4b). Interestingly, the temporal patterns of HIX_{WSBrC} and $HIX_{WI-MSBrC}$ were found to be similar with relatively stable in summer followed by a sharp increase in early autumn and then a gradual decrease to summer through winter and spring (Fig. 4c). Further the HIX_{WSBrC} was always significantly higher than the $HIX_{WI-MSBrC}$. Such temporal differences in all the three fluorescence indices clearly indicate that the composition and/or aromaticity of WSBrC and WI-MSBrC are substantially distinct, even though they might have been mainly derived from similar sources: biomass burning and coal combustion, as discussed in previous section.

Average FI_{WSBrC} was found to be higher in autumn followed the similar levels in winter and spring and the lowest in summer, whereas that of BIX_{WSBrC} was higher in winter followed by autumn, spring and the lowest in summer (Table 1). While the averages of both $FI_{WI-MSBrC}$ and $BIX_{WI-MSBrC}$ were higher in winter followed by summer, spring and the lowest in autumn (Table 1). Annual and seasonal averages of FI values of both WSBrC and WI-MSBrC were around or higher than 1.4 and lower than 1.9 in Tianjin, indicating that the BrC in Tianjin was mainly derived from terrestrial OM that should have largely consist of high aromatic compounds. In contrast, the annual and seasonal averages of BIX of both WSBrC and WI-MSBrC were higher than 1.0 (Table 1), indicating the predominant contributions of OM from the biological (including biomass burning) sources. In addition, the lowest FI_{WSBrC} and BIX_{WSBrC} values in summer and those of the $FI_{WI-MSBrC}$ in spring and $BIX_{WI-MSBrC}$ in autumn suggest that the contribution from terrestrial sources (e.g., coal combustion) might be less in spring and autumn and the photobleaching of OA might be significant under high solar radiation in summer.

HIX_{WSBrC} and $HIX_{WI-MSBrC}$ were ranged from 1.72 to 4.7 with an average of 2.87 and 0.11−2.38 (avg. 0.81), respectively, during the campaign, which again support that both the BrC components in Tianjin should have been significantly derived from biomass burning and might consist highly humified and aromatic compounds. Average HIX_{WSBrC} was higher in summer followed by autumn, spring and the lowest in winter (Table 1). In contrast, the average $HIX_{WI-MSBrC}$ was higher in winter followed by autumn, spring and the lowest in summer (Table 1). It has been reported that aging processes and HIX have a significant relation (Deng et al., 2022). The higher HIX_{WSBrC} and lower $HIX_{WI-MSBrC}$ in summer confirm that the BrC, which is more water-soluble, was significantly produced from aromatic compounds and subjected for significant atmospheric aging in summer over the Tianjin region.
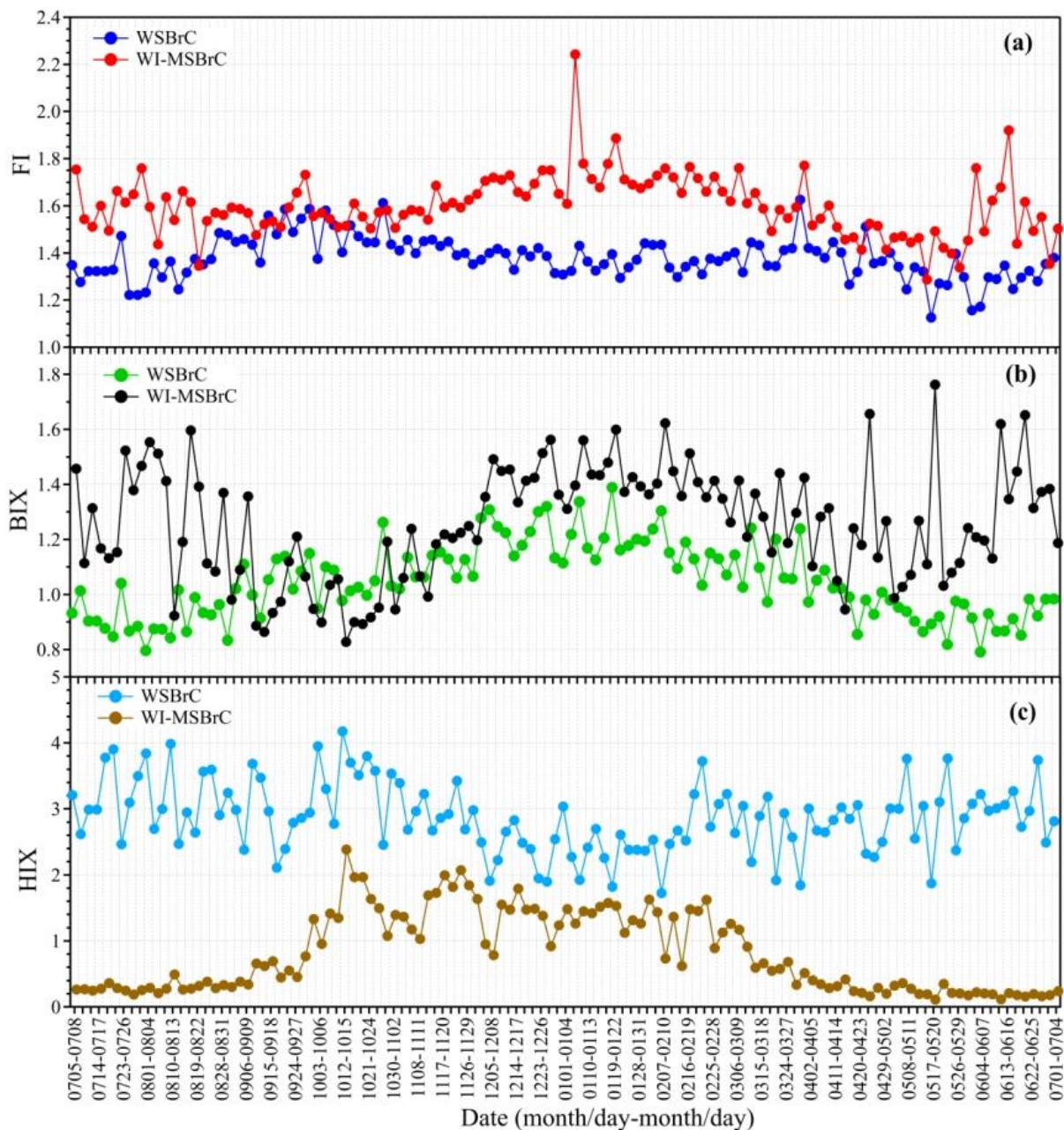
Figure 4. Temporal variations in light absorption and fluorescence properties of BrC in $PM_{2.5}$ Tianjin: (a) FI, (b) BIX, and (c) HIX.

3.3.2 Fluorophore identification

It is well established that fluorophores with different excitation emission wavelengths can distinguish their types and sources. However, the types and sources of a large number of fluorophores have not been determined due to their complex chemical composition and sources. Here, we separated several fluorescence components from the EEM data using the parallel factor analysis (PARAFAC) model, and the results are shown in Fig. 5. The fact of the value of core consistency close to 100 in PARAFAC model indicates that the more the individual components

17

that are analyzed together make up 100% of the mixture, with no unexplained residues. The core consistency of PARAFAC model explained the maximum variance of 89% for WSBrC and of 95% for WI-MSBrC whole data obtained during the campaign, when three independent groups were chosen for the simulation.
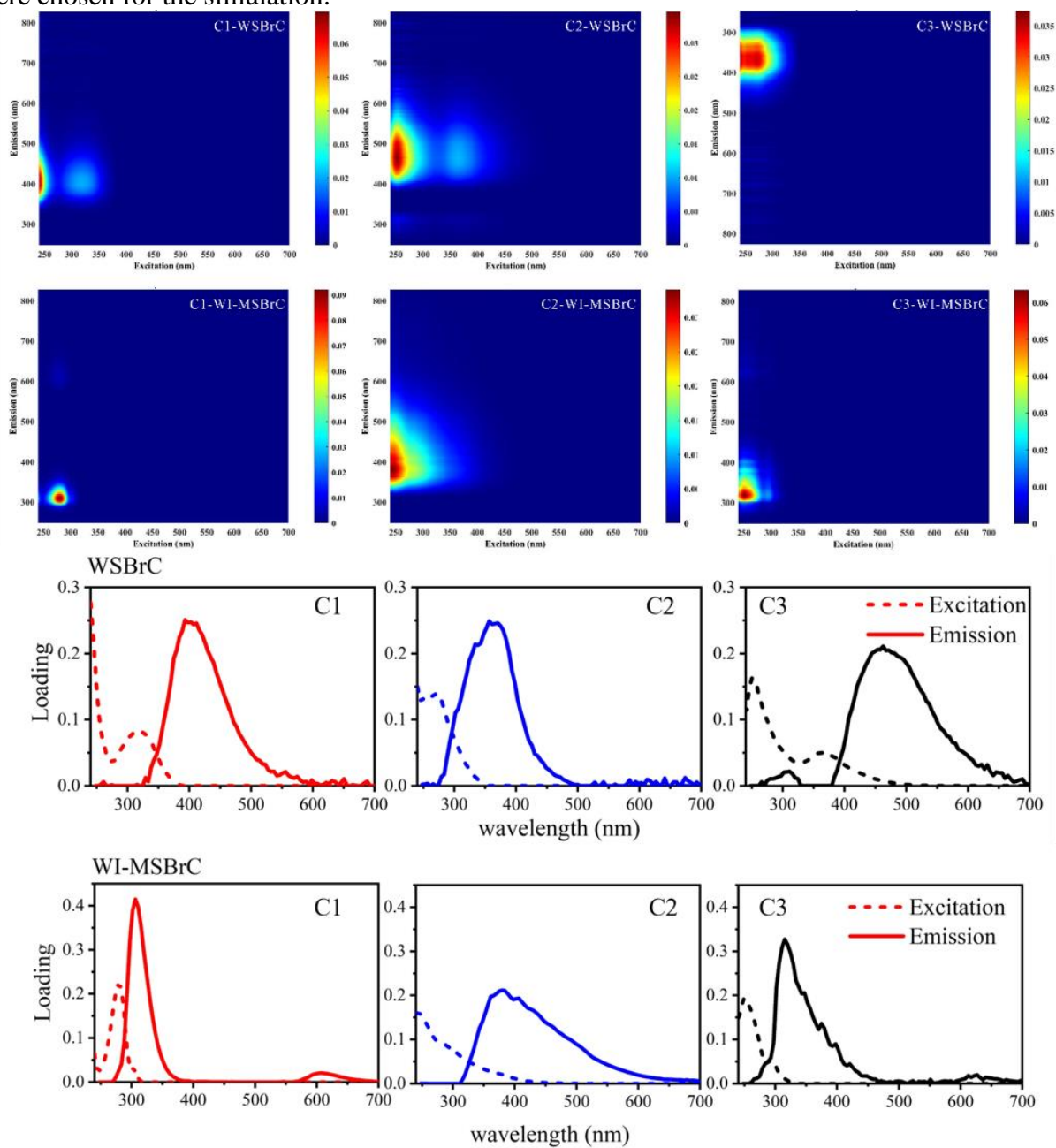
Figure 5. Three-dimensional excitation-emission matrix of three fluorescent components (upper panel) together with their excitation and emission loadings (lower panel) of WSBrC and WI-MSBrC obtained by PARAFAC model analysis.

The types of fluoroophores of both WSBrC and WI-MSBrC identified in this study together with their excitation and emission wavelengths and those reported in the literature are summarized

581 in Table 2. Among the total of three types of fluorophores obtained for WSBrC in Tianjin $PM_{2.5}$
582 by PARAFAC for EEMs, two showed the fluorescence characteristics similar to those of less
583 oxygenated and highly oxygenated humic-like substances (HULIS), respectively, and the third one
584 showed similar to those of protein compounds (PLOM). Fluorophore C1$_{WSBrC}$ has a primary
585 fluorescence peak at excitation/emission (Ex/Em): <240/393 nm, and a secondary fluorescence
586 peak at Ex/Em: 318/393 nm. C1$_{WSBrC}$ can be classified as a humus-like fluorophore because the
587 bimodal distribution of the fluorescence spectrum is usually associated with HULIS. The emission
588 wavelength of C1$_{WSBrC}$ was closer to the UV region than that of the second peak of C2$_{WSBrC}$,
589 indicating the existence of a small number of aromatic substances, conjugate systems and
590 nonlinear ring systems (Deng et al., 2022). C2$_{WSBrC}$ (Ex/Em ~251, 363 nm/462 nm) was identified
591 as a common HULIS in aerosols, with higher oxidation, aromatization, molecular weight,
592 conjugation, and unsaturation due to its larger emission wavelength (Wen et al., 2021). The
593 molecular weight of the fluorophore as well as its degree of conjugation tend to increase with the
594 excitation wavelength, and such increase in size and the conjugation degree may be attributed to
595 the presence of highly aromatic conjugated structures containing heteroatoms (Chen et al., 2019).
596 Compared to C1$_{WSBrC}$ and C2$_{WSBrC}$, C3$_{WSBrC}$ also contains two peaks, with shorter wavelengths
597 (<380 nm) emission peak, which is usually associated with protein-like organic matter (PLOM)
598 such as tryptophan and tyrosine, with low aromatic properties and small molecular size (Table 2).
599
600 **Table 2.** Description and wavelength positions of PARAFAC components in this study and other
601 reports from the literature. (PLOM = protein compounds; HULIS = humic-like substances)

Category	Components	Ex(nm)	Em(nm)	Substances	References
WSBrC	C1	<240, 318	393	low-oxygenated HULIS	
	C2	251, 363	462	high-oxygenated HULIS	
	C3	<240, 271	356.3	PLOM, such as tryptophan and tyrosine	this study
WI-MSBrC	C1	<240, 279	306	PLOM, tyrosine-like	
	C2	<240	379	uncertain	
	C3	251, 294	315	PLOM, tryptophan-like	
Water-soluble BrC	C1	250, 315	396	low-oxygenated HULIS	
	C2	250	465	highly-oxygenated HULIS	
	C3	250	385	low-oxygenated HULIS	(Deng et al., 2022)
	C4	250	340	PLOM, tryptophan-like	
	C5	275	305	PLOM, tyrosine-like	
WSOC	C1	240, 315	393	low-oxygenated HULIS	
	C2	245, 360	476	highly-oxygenated HULIS	(Wen et al., 2021)
	C3	<240, 290	361	PLOM, such as tryptophan and tyrosine	
	C4	275	311	PLOM, tyrosine-like	
WSM and MSM	C1	255	415	HULIS-1 component	
	C2	220	340	tryptophan-like component	
	C3	255	385	HULIS-2 component	(Chen et al., 2019)
	C4	210	300	tyrosine-like component	
	C5	250	355	amino acid-like component	
WSOC	C1	245	410	HULIS, photodegradation of macromolecules	
	C2	235	398	HULIS, aromatic and saturated compounds were presented	
	C3	250, 360	466	humic-like chromophores, more aromatic and consisted of more unsaturated compounds produced by condensation reactions	(Xie et al., 2020)
	C4	250, 285	432	terrestrial humic-like chromophore	
	C5	<235	430	terrestrial humic-like substance, photochemical product	
MSOC	C6	275	408	low oxidation humic-like	
	C7	235, 275	372	protein-like chromophore	
	C8	260, 310	364	protein-like (tryptophan-like), may be related to PAHs	

602

However, WI-MSBrC fluorophore C1$_{\text{WI-MSBrC}}$ might be tyrosine-like substance. C2$_{\text{WI-MSBrC}}$ is not quite certain and could be either HULIS or PLOM, because its emission wavelength <380 nm generally fits the profile of PLOM, but it is also close to the emission wavelength of HULIS. While C3$_{\text{WI-MSBrC}}$ is a tryptophan-like substance, which was reported to contain less aromatic and small molecular weight compounds. In general, phenols contribute significantly to C3$_{\text{WI-MSBrC}}$ fluorophore as they are the products of incomplete pyrolysis of lignin and cellulose and are used as indicators of biomass burning (Wen et al., 2021). Therefore, WI-MSBrC fluorophores of all samples in this study can be classified as mainly PLOM.

The percent contributions of each fluorophore to WSBrC and WI-MSBrC in PM$_{2.5}$ in Tianjin in each season are shown in Fig. 6. The compositions of WSBrC and WI-BrC clearly imply that the former contained more HULIS, whereas the later consist mostly of PLOM, and also indicate that most of the fluorophores of protein-like substances could dissolve in organic solvent, rather than in water.

According to the excitation emission wavelength, we classified the fluorescence component of WI-MSBrC substance as PLOM, but the correlation between their fluorescence intensity and BIX (R = 0.66, $p < 0.05$) was very small, far lower than that of WSBrC substance and BIX (R = 0.59, $p < 0.05$). On the contrary, the correlation between their fluorescence intensity and HIX (R = 0.74, $p < 0.05$) was much higher than that of WSBrC (R = –0.10, $p < 0.05$). Although PLOM may be associated with some polycyclic aromatic hydrocarbons (PAHs) or phenols from fossil fuel combustion and biomass burning, especially in urban aerosols, the correlation is puzzling.
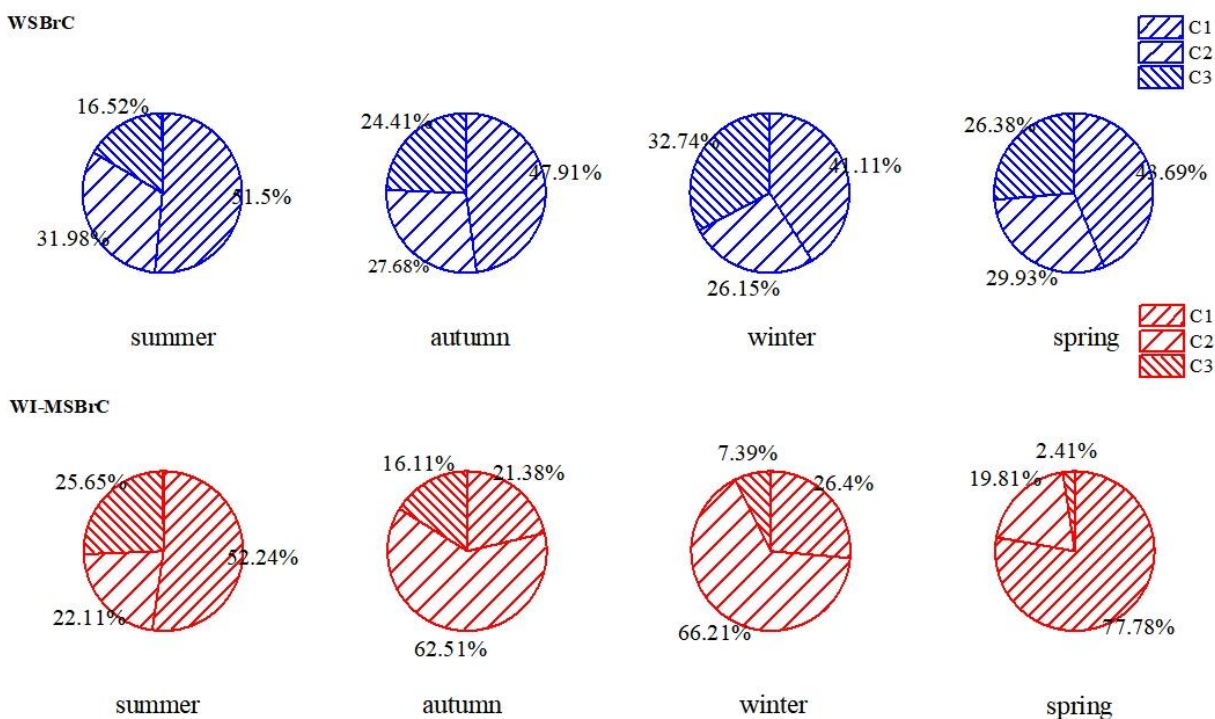
**Figure 6**. Relative abundances of the chromophores of the WSBrC and WI-MSBrC in PM$_{2.5}$ from Tianjin.

On average, the humic-like fluorophores together contributed more than 60% to the fluorescence intensity in WSBrC, suggesting that humic-like fluorophores played a dominant role

in fluorescence properties of WSBrC in Tianjin. Generally, the low-oxygenated fluorophores C1$_{WSBrC}$ made considerable contributions in each season. While C2$_{WSBrC}$, highly oxygenated HULIS, has a greater relative contribution in summer, which might be due to the strong solar radiation in summer. In contrast, in WI-MSBrC, the average contribution of PLOM to fluorescence intensity was higher than 70% in spring (80.2%) and summer (77.9%), but C2$_{WI-MSBrC}$ component dominated in winter and autumn. This indicated that biological activities increased in spring and summer and the relative abundance of bioaerosols might be higher during that period.

3.4 Potential sources of BrC

To further explore the potential sources of BrC, correlations of FV with chemical components and light absorption of PM$_{2.5}$ were examined. The sum of FVs of WSBrC and WI-MSBrC (FVs$_{(WSBrC+WI-MSBrC)}$) showed a significant correlation with secondary OC (SOC) in autumn (R = 0.90, $p < 0.05$) and winter (R = 0.67, $p < 0.05$). Furthermore, the correlation between FVs$_{(WSBrC+WI-MSBrC)}$ and EC in each season was insignificant. Such relations suggest that the secondary formation processes should have been played an important role in controlling the loadings of BrC in autumn and winter as well. A good correlation between FV and Abs$_{365}$ of both WSBrC and WI-MSBrC was found in all seasons except winter, which indicates that most light-absorbing materials would also have significant fluorescence characteristics.

The relative contents of different chromophores in different polar extracts depend on their sources and varied significantly. The results showed that the NFVs of WSBrC were lower than those the WI-MSBrC and were different from season to season in Tianjin (Fig. 7). Recently, it has been reported that the aerosols derived from biomass burning and coal combustion exhibit the highest NFV values, while SOA show the lowest NFV values (Chen et al., 2020). NFV in all samples studied in Tianjin during 2018–2019 was very similar to that of primary emissions and higher than that of secondary aerosols. Such result reveal that the fluorophores in the Tianjin PM$_{2.5}$ might mainly be derived from a primary combustion sources as well. In addition, the NFVs of the Tianjin PM$_{2.5}$ were higher in winter than in summer, which is likely and can be attributed to the photolysis of chromophores in summer. In addition, NFV of WI-MSBrC was much higher than that in WSBrC, which indicate that fluorescence contribution of fluorophores was abundant in WI-MSBrC than in the WSBrC.
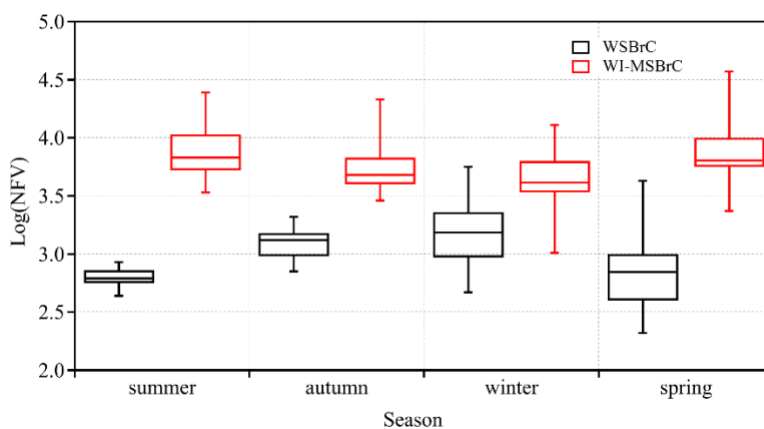
Figure 7. The normalized fluorescence volumes (NFVs) of the WSBrC and WI-MSBrC of PM$_{2.5}$ from Tianjin, North China.

4. Summary and Conclusions

This study presents the temporal variations in light absorption and fluorescence properties of water-soluble BrC (WSBrC) and the water-insoluble but MeOH-soluble BrC (WI-MSBrC) in $PM_{2.5}$ collected from Tianjin, North China during July 5, 2018 – July 5, 2019. Light absorption properties of WSBrC and WI-MSBrC in Tianjin were investigated and found to be distinct from season to season, which was lower in spring and summer, compared with that in autumn and winter. The AAE of WI-MSBrC was comparable with that of WSBrC. The mass absorption efficiency of WSBrC and WI-MSBrC (MAE_{365}) exhibited distinct seasonal variations, which was higher in winter and lower in summer and autumn. Biologically derived or secondary BrC and/or its photobleaching might be the reasons for the lower MAE_{365} values in summer and autumn. The light absorption of both WSBrC and WI-MSBrC in the range of 300–400 nm to that in the whole range (300–700 nm) was ~40%, indicating that BrC in the UV-Vis range plays an important role in climate warming. In addition, based on PARAFAC analysis model, EEM data were comprehensively analyzed to identify the types and abundance of different fluorophores, and obtained three types of the fluorophores: low-oxygenated HULIS, high-oxygenated HULIS and protein-like compound (PLOM). The correlation between BrC optical properties and aerosol chemical composition indicated that biomass burning, and fossil fuel (mainly coal) combustion significantly contributed to BrC content in winter, while primary biological emission and subsequent aging significantly contributed to the BrC content in summer. These results illustrated the light absorption properties of BrC in metropolis aerosols and emphasized its significant contribution to radiative forcing.

Declaration of competing intertest

The authors declare no competing intertest in this paper.

Data Availability Statement

The data used in this study can be found online at https://doi.org/10.5281/zenodo.7316371 (Dong et al., 2022), and at https://doi.org/10.5281/zenodo.5140861 (Dong et al., 2021).

Supplement.

The supplement related to this article is available online at:

Acknowledgments

References

Andreae, M. O., and Gelencs´er, A.: Black carbon or brown carbon? The nature of light-absorbing carbonaceous aerosols, Atmospheric Chemistry and Physics, 6, 3131–3148, www.atmos-chem-phys.net/6/3131/2006/, 2006.

Baduel, C., Voisin, D., and Jaffrezo, J. L.: Comparison of analytical methods for Humic Like Substances (HULIS) measurements in atmospheric particles, Atmospheric Chemistry and Physics, 9, 5949-5962, 10.5194/acp-9-5949-2009, 2009.

Battin, T. J.: Dissolved organic matter and its optical properties in a blackwater tributary of the upper Orinoco river, Venezuela, Organic Geochemistry, 28, 561-569, https://doi.org/10.1016/S0146-6380(98)00028-X, 1998.

Birdwell, J. E., and Engel, A. S.: Characterization of dissolved organic matter in cave and spring waters using UV-Vis absorbance and fluorescence spectroscopy, Org Geochem, 41, 270-280, 10.1016/j.orggeochem.2009.11.002, 2010.

Bond, T. C., and Bergstrom, R. W.: Light absorption by carbonaceous particles: An investigative review, Aerosol Science and Technology, 40, 27-67, 10.1080/02786820500421521, 2006.

Brown, H., Liu, X., Pokhrel, R., Murphy, S., Lu, Z., Saleh, R., Mielonen, T., Kokkola, H., Bergman, T., Myhre, G., Skeie, R. B., Watson-Paris, D., Stier, P., Johnson, B., Bellouin, N., Schulz, M., Vakkari, V., Beukes, J. P., van Zyl, P. G., Liu, S., and Chand, D.: Biomass burning aerosols in most climate models are too absorbing, Nature Communications, 12, 277, 10.1038/s41467-020-20482-9, 2021.

Cao, T., Li, M., Xu, C., Song, J., Fan, X., Li, J., Jia, W., and Peng, P.: Technical note: Identification of chemical composition and source of fluorescent components in atmospheric water-soluble brown carbon by excitation-emission matrix with parallel factor analysis: Potential limitation and application, Atmospheric Chemistry and Physics Discussions, 2022, 1-41, 10.5194/acp-2022-676, 2022.

Chen, Q., Fumikazu, I., Hayato, H., Daichi, A., and Michihiro, M.: Chemical structural characteristics of HULIS and other fractionated organic matter in urban aerosols: Results from mass spectral and FT-IR analysis, Environmental Science & Technology, 50, 1721-1730, 10.1021/acs.est.5b05277, 2016a.

Chen, Q., Miyazaki, Y., Kawamura, K., Matsumoto, K., Coburn, S., Volkamer, R., Iwamoto, Y., Kagami, S., Deng, Y., Ogawa, S., Ramasamy, S., Kato, S., Ida, A., Kajii, Y., and Mochida, M.: Characterization of chromophoric water-soluble organic matter in urban, forest, and marine aerosols by HR-ToF-AMS analysis and excitation–emission matrix spectroscopy, Environmental Science & Technology, 50, 10351-10360, 10.1021/acs.est.6b01643, 2016b.

Chen, Q., Mu, Z., Song, W., Wang, Y., Yang, Z., Zhang, L., and Zhang, Y.-L.: Size-resolved characterization of the chromophores in atmospheric particulate matter from a typical coal-burning city in China, Journal of Geophysical Research: Atmospheres, 124, 10546-10563, https://doi.org/10.1029/2019JD031149, 2019.

Chen, Q., Li, J., Hua, X., Jiang, X., Mu, Z., Wang, M., Wang, J., Shan, M., Yang, X., Fan, X., Song, J., Wang, Y., Guan, D., and Du, L.: Identification of species and sources of atmospheric chromophores by fluorescence excitation-emission matrix with parallel factor analysis, Science of the Total Environment, 718, 137322, 10.1016/j.scitotenv.2020.137322, 2020.

Chen, Q. C., Ikemori, F., and Mochida, M.: Light Absorption and Excitation-Emission Fluorescence of Urban Organic Aerosol Components and Their Relationship to Chemical Structure, Environ Sci Technol, 50, 10859-10868, 10.1021/acs.est.6b02541, 2016c.

Choudhary, V., Rajput, P., and Gupta, T.: Absorption properties and forcing efficiency of light-absorbing water-soluble organic aerosols: Seasonal and spatial variability, Environ Pollut, 272, ARTN 115932 10.1016/j.envpol.2020.115932, 2021.

Coble, P. G.: Marine optical biogeochemistry: The chemistry of ocean color, Chem Rev, 107, 402-418, 10.1021/cr050350+, 2007.

Corbin, J. C., Czech, H., Massabò, D., de Mongeot, F. B., Jakobi, G., Liu, F., Lobo, P., Mennucci, C., Mensah, A. A., Orasche, J., Pieber, S. M., Prévôt, A. S. H., Stengel, B., Tay, L. L., Zanatta, M., Zimmermann, R., El Haddad, I.,

746   and Gysel, M.: Infrared-absorbing carbonaceous tar can dominate light absorption by marine-engine exhaust, npj
747   Climate and Atmospheric Science, 2, 12, 10.1038/s41612-019-0069-5, 2019.
748   Deng, J., Ma, H., Wang, X., Zhong, S., Zhang, Z., Zhu, J., Fan, Y., Hu, W., Wu, L., Xiaodong, L., Ren, L., Pavuluri,
749   C. M., Pan, X., Sun, Y., Wang, Z., Kawamura, K., and Fu, P.: Measurement Report: Optical properties and sources
750   of water-soluble brown carbon in Tianjin, North China: insights from organic molecular compositions, Atmospheric
751   Chemistry and Physics, 22, 6449-6470, 10.5194/acp-2021-1045, 2022.
752   Diggs, D. L., Huderson, A. C., Harris, K. L., Myers, J. N., Banks, L. D., Rekhadevi, P. V., Niaz, M. S., and Ramesh,
753   A.: Polycyclic aromatic hydrocarbons and digestive tract cancers: a perspective, Journal of Environmental Science
754   and Health, Part C, 29, 324-357, 10.1080/10590501.2011.629974, 2011.
755   Dong, Z., Pavuluri, C. M., Xu, Z., Wang, Y., Li, P., Fu, P., and Liu, C. Q.: Measurement report: Chemical
756   components and 13C and 15N isotope ratios of fine aerosols over Tianjin, North China: year-round observations,
757   Atmospheric Chemistry and Physics, 23, 2119-2143, 10.5194/acp-23-2119-2023, 2023a.
758   Dong, Z. C., Pavuluri, C. M., Xu, Z. J., Wang, Y., Li, P. S., Fu, P. Q., and Liu, C. Q.: Year-round observations of
759   bulk components and 13C and 15N isotope ratios of fine aerosols at Tianjin, North China – Data set. 2021.
760   Dong, Z. C., Pavuluri, C. M., Li, P. S., Xu, Z. J., Deng, J. J., Zhao, X. Y., and Zhao, X. M.: Year-round observations
761   of the optical properties of brown carbon in fine aerosols at Tianjin, North China – Data set. 2022.
762   Dong, Z. C., Pavuluri, C. M., Xu, Z. J., Wang, Y., Li, P. S., Fu, P. Q., and Liu, C. Q.: Measurement report:
763   Chemical components and
764   C and
765   N isotoperatios of fine aerosols over Tianjin, North China: year-round observations, Atmos Chem Phys, 23, 2119-
766   2143, 10.5194/acp-23-2119-2023, 2023b.
767   Fan, X. J., Wei, S. Y., Zhu, M. B., Song, J. Z., and Peng, P. A.: Comprehensive characterization of humic-like
768   substances in smoke PM
769   emitted from the combustion of biomass materials and fossil fuels, Atmos Chem Phys, 16, 13321-13340,
770   10.5194/acp-16-13321-2016, 2016.
771   Feng, Y., Ramanathan, V., and Kotamarthi, V. R.: Brown carbon: a significant atmospheric absorber of solar
772   radiation?, Atmospheric Chemistry and Physics Discussions, 10.5194/acpd-13-2795-2013, 2013.
773   Gao yan, and Zhang, y.: Formation and photochemical investigation of brown carbon by hydroxyacetone reactions
774   with glycine and ammonium sulfate, Royal Society of Chemistry Advances, 8, 20719-20725,
775   10.1039/C8RA02019A, 2018.
776   Gu, Q., and Kenny, J. E.: Improvement of inner filter effect correction based on determination of effective geometric
777   parameters using a conventional fluorimeter, Analytical Chemistry, 81, 420-426, 10.1021/ac801676j, 2009.
778   Hecobian, A., Zhang, X., Zheng, M., Frank, N., Edgerton, E. S., and Weber, R. J.: Water-Soluble Organic Aerosol
779   material and the light-absorption characteristics of aqueous extracts measured over the Southeastern United States,
780   Atmospheric Chemistry and Physics, 10, 5965-5977, 10.5194/acp-10-5965-2010, 2010.
781   Hems, R. F., Schnitzler, E. G., Liu-Kang, C., Cappa, C. D., and Abbatt, J. P. D.: Aging of atmospheric brown carbon
782   aerosol, ACS Earth and Space Chemistry, 5, 722-748, 10.1021/acsearthspacechem.0c00346, 2021.
783   Hoffer, A., Gelencsér, A., Guyon, P., Kiss, G., Schmid, O., Frank, G. P., Artaxo, P., and Andreae, M. O.: Optical
784   properties of humic-like substances (HULIS) in biomass-burning aerosols, Atmospheric Chemistry and Physics, 6,
785   3563-3570, 10.5194/acp-6-3563-2006, 2006.
786   Huang, R. J., Yang, L., Cao, J., Chen, Y., Chen, Q., Li, Y., Duan, J., Zhu, C., Dai, W., Wang, K., Lin, C., Ni, H.,
787   Corbin, J. C., Wu, Y., Zhang, R., Tie, X., Hoffmann, T., O'Dowd, C., and Dusek, U.: Brown carbon aerosol in urban
788   Xi'an, Northwest China: The composition and light absorption properties, Environmental Science & Technology,
789   52, 6825-6833, 10.1021/acs.est.8b02386, 2018.
790   Huang, R. J., Yang, L., Shen, J., Yuan, W., Gong, Y., Guo, J., Cao, W., Duan, J., Ni, H., Zhu, C., Dai, W., Li, Y.,
791   Chen, Y., Chen, Q., Wu, Y., Zhang, R., Dusek, U., O'Dowd, C., and Hoffmann, T.: Water-insoluble organics
792   dominate brown carbon in wintertime urban aerosol of China: Chemical characteristics and optical properties,
793   Environmental Science & Technology, 54, 7836-7847, 10.1021/acs.est.0c01149, 2020.
794   Jo, D. S., Park, R. J., Lee, S., Kim, S. W., and Zhang, X.: A global simulation of brown carbon: implications for
795   photochemistry and direct radiative effect, Atmospheric Chemistry and Physics, 16, 3413-3432, 10.5194/acp-16-
796   3413-2016, 2016.
797   Kasthuriarachchi, N. Y., Rivellini, L.-H., Chen, X., Li, Y. J., and Lee, A. K. Y.: Effect of relative humidity on
798   secondary brown carbon formation in aqueous droplets, Environmental Science & Technology, 54, 13207-13216,
799   10.1021/acs.est.0c01239, 2020.

800 Lack, D. A., Bahreni, R., Langridge, J. M., Gilman, J. B., and Middlebrook, A. M.: Brown carbon absorption linked
801 to organic mass tracers in biomass burning particles, Atmospheric Chemistry and Physics, 13, 2415-2422,
802 10.5194/acp-13-2415-2013, 2013.
803 Laskin, A., Laskin, J., and Nizkorodov, S. A.: Chemistry of Atmospheric Brown Carbon, Chem Rev, 115, 4335-
804 4382, 10.1021/cr5006167, 2015a.
805 Laskin, A., Laskin, J., and Nizkorodov, S. A.: Chemistry of atmospheric brown carbon, Chemical Reviews, 115,
806 4335-4382, 10.1021/cr5006167, 2015b.
807 Lawaetz, A. J., and Stedmon, C. A.: Fluorescence intensity calibration using the Raman scatter peak of water,
808 Applied Spectroscopy, 63, 936-940, 10.1366/000370209788964548, 2009.
809 Lee, H. J., Laskin, A., Laskin, J., and Nizkorodov, S. A.: Excitation-Emission Spectra and Fluorescence Quantum
810 Yields for Fresh and Aged Biogenic Secondary Organic Aerosols, Environ Sci Technol, 47, 5763-5770,
811 10.1021/es400644c, 2013.
812 Lesworth, T., Baker, A. R., and Jickells, T.: Aerosol organic nitrogen over the remote Atlantic Ocean, Atmospheric
813 Environment, 44, 1887-1893, https://doi.org/10.1016/j.atmosenv.2010.02.021, 2010.
814 Li, C., He, Q., Hettiyadura, A. P. S., Käfer, U., Shmul, G., Meidan, D., Zimmermann, R., Brown, S. S., George, C.,
815 Laskin, A., and Rudich, Y.: Formation of secondary brown carbon in biomass burning aerosol proxies through NO3
816 radical reactions, Environmental Science & Technology, 54, 1395-1405, 10.1021/acs.est.9b05641, 2020a.
817 Li, J., Zhang, Q., Wang, G., Li, J., Wu, C., Liu, L., Wang, J., Jiang, W., Li, L., Ho, K. F., and Cao, J.: Optical
818 properties and molecular compositions of water-soluble and water-insoluble brown carbon (BrC) aerosols in
819 northwest China, Atmospheric Chemistry and Physics, 20, 4889-4904, 10.5194/acp-20-4889-2020, 2020b.
820 Li, S., Zhu, M., Yang, W. Q., Tang, M. J., Huang, X. L., Yu, Y. G., Fang, H., Yu, X., Yu, Q. Q., Fu, X. X., Song,
821 W., Zhang, Y. L., Bi, X. H., and Wang, X. M.: Filter-based measurement of light absorption by brown carbon in
822 PM2.5 in a megacity in South China, Science of the Total Environment, 633, 1360-1369,
823 10.1016/j.scitotenv.2018.03.235, 2018.
824 Li, X., Fu, P., Tripathee, L., Yan, F., Hu, Z., Yu, F., Chen, Q., Li, J., Chen, Q., Cao, J., and Kang, S.: Molecular
825 compositions, optical properties, and implications of dissolved brown carbon in snow/ice on the Tibetan Plateau
826 glaciers, Environment International, 164, 107276, https://doi.org/10.1016/j.envint.2022.107276, 2022.
827 Liakakou, E., Kaskaoutis, D. G., Grivas, G., Stavroulas, I., Tsagkaraki, M., Paraskevopoulou, D., Bougiatioti, A.,
828 Dumka, U. C., Gerasopoulos, E., and Mihalopoulos, N.: Long-term brown carbon spectral characteristics in a
829 Mediterranean city (Athens), Sci Total Environ, 708, 135019, 10.1016/j.scitotenv.2019.135019, 2020.
830 Lin, G., Penner, J. E., Flanner, M. G., Sillman, S., Xu, L., and Zhou, C.: Radiative forcing of organic aerosol in the
831 atmosphere and on snow: Effects of SOA and brown carbon, Journal of Geophysical Research: Atmospheres, 119,
832 7453-7476, 10.1002/2013jd021186, 2014.
833 Lin, P., Bluvshtein, N., Rudich, Y., Nizkorodov, S. A., Laskin, J., and Laskin, A.: Molecular Chemistry of
834 Atmospheric Brown Carbon Inferred from a Nationwide Biomass Burning Event, Environ Sci Technol, 51, 11561-
835 11570, 10.1021/acs.est.7b02276, 2017.
836 Liu, J., Bergin, M., Guo, H., King, L., Kotra, N., Edgerton, E., and Weber, R. J.: Size-resolved measurements of
837 brown carbon in water and methanol extracts and estimates of their contribution to ambient fine-particle light
838 absorption, Atmospheric Chemistry and Physics, 13, 12389-12404, 10.5194/acp-13-12389-2013, 2013.
839 McKnight, D. M., Boyer, E. W., Westerhoff, P. K., Doran, P. T., Kulbe, T., and Andersen, D. T.:
840 Spectrofluorometric Characterization of Dissolved Organic Matter for Indication of Precursor Organic Material and
841 Aromaticity, Limnology and Oceanography, 46, 38-48, 2001.
842 Murphy, K. R., Stedmon, C. A., Graeber, D., and Bro, R.: Fluorescence spectroscopy and multi-way techniques.
843 PARAFAC, Analytical Methods, 5, 6557-6566, 10.1039/C3AY41160E, 2013.
844 Park, R. J., Kim, M. J., Jeong, J. I., Youn, D., and Kim, S.: A contribution of brown carbon aerosol to the aerosol
845 light absorption and its radiative forcing in East Asia, Atmospheric Environment, 44, 1414-1421,
846 10.1016/j.atmosenv.2010.01.042, 2010.
847 Peters, S., Talaska, G., Jonsson, B. A., Kromhout, H., and Vermeulen, R.: Polycyclic aromatic hydrocarbon
848 exposure, urinary mutagenicity, and DNA adducts in rubber manufacturing workers, Cancer Epidemiol Biomarkers
849 Prev, 17, 1452-1459, 10.1158/1055-9965.EPI-07-2777, 2008.
850 Qin, J., Zhang, L., Zhou, X., Duan, J., Mu, S., Xiao, K., Hu, J., and Tan, J.: Fluorescence fingerprinting properties
851 for exploring water-soluble organic compounds in PM2.5 in an industrial city of northwest China, Atmospheric
852 Environment, 184, 203-211, https://doi.org/10.1016/j.atmosenv.2018.04.049, 2018.
853 Rizzo, L. V., Correia, A. L., Artaxo, P., Procópio, A. S., and Andreae, M. O.: Spectral dependence of aerosol light
854 absorption over the Amazon Basin, Atmospheric Chemistry and Physics, 11, 8899-8912, 10.5194/acp-11-8899-
855 2011, 2011.

856 Rizzo, L. V., Artaxo, P., Müller, T., Wiedensohler, A., Paixão, M., Cirino, G. G., Arana, A., Swietlicki, E., Roldin,
857 P., Fors, E. O., Wiedemann, K. T., Leal, L. S. M., and Kulmala, M.: Long term measurements of aerosol optical
858 properties at a primary forest site in Amazonia, Atmos. Chem. Phys., 13, 2391-2413, 10.5194/acp-13-2391-2013,
859 2013.
860 Saleh, R.: From Measurements to Models: Toward Accurate Representation of Brown Carbon in Climate
861 Calculations, Current Pollution Reports, 6, 90-104, 10.1007/s40726-020-00139-3, 2020.
862 Shamjad, P. M., Tripathi, S. N., Thamban, N. M., and Vreeland, H.: Refractive Index and Absorption Attribution of
863 Highly Absorbing Brown Carbon Aerosols from an Urban Indian City-Kanpur, Sci Rep-Uk, 6, 10.1038/srep37735,
864 2016.
865 Shetty, N. J., Pandey, A., Baker, S., Hao, W. M., and Chakrabarty, R. K.: Measuring light absorption by freshly
866 emitted organic aerosols: optical artifacts in traditional solvent-extraction-based methods, Atmos. Chem. Phys., 19,
867 8817-8830, 10.5194/acp-19-8817-2019, 2019.
868 Sun, J., Zhi, G., Hitzenberger, R., Chen, Y., Tian, C., Zhang, Y., Feng, Y., Cheng, M., Zhang, Y., Cai, J., Chen, F.,
869 Qiu, Y., Jiang, Z., Li, J., Zhang, G., and Mo, Y.: Emission factors and light absorption properties of brown carbon
870 from household coal combustion in China, Atmos. Chem. Phys., 17, 4769-4780, 10.5194/acp-17-4769-2017, 2017.
871 Tang, J., Li, J., Mo, Y., Safaei Khorram, M., Chen, Y., Tang, J., Zhang, Y., Song, J., and Zhang, G.: Light
872 absorption and emissions inventory of humic-like substances from simulated rainforest biomass burning in
873 Southeast Asia, Environmental Pollution, 262, 114266, https://doi.org/10.1016/j.envpol.2020.114266, 2020.
874 Wang, D., Shen, Z., Zhang, Q., Lei, Y., Zhang, T., Huang, S., Sun, J., Xu, H., and Cao, J.: Winter brown carbon
875 over six of China's megacities: light absorption, molecular characterization, and improved source apportionment
876 revealed by multilayer perceptron neural network, Atmospheric Chemistry and Physics, 22, 14893-14904,
877 10.5194/acp-22-14893-2022, 2022a.
878 Wang, Q. Q., Zhou, Y. Y., Ma, N., Zhu, Y., Zhao, X. C., Zhu, S. W., Tao, J. C., Hong, J., Wu, W. J., Cheng, Y. F.,
879 and Su, H.: Review of brown carbon aerosols in China: Pollution level, optical properties, and emissions, Journal of
880 Geophysical Research: Atmospheres, 127, 10.1029/2021JD035473, 2022b.
881 Wang, Y., Pavuluri, C. M., Fu, P., Li, P., Dong, Z., Xu, Z., Ren, H., Fan, Y., Li, L., Zhang, Y.-L., and Liu, C.-Q.:
882 Characterization of Secondary Organic Aerosol Tracers over Tianjin, North China during Summer to Autumn, ACS
883 Earth and Space Chemistry, 3, 2339-2352, 10.1021/acsearthspacechem.9b00170, 2019.
884 Wen, H., Zhou, Y., Xu, X., Wang, T., Chen, Q., Chen, Q., Li, W., Wang, Z., Huang, Z., Zhou, T., Shi, J., Bi, J., Ji,
885 M., and Wang, X.: Water-soluble brown carbon in atmospheric aerosols along the transport pathway of Asian dust:
886 Optical properties, chemical compositions, and potential sources, Science of the Total Environment, 789, 147971,
887 10.1016/j.scitotenv.2021.147971, 2021.
888 Wu, G., Fu, P., Ram, K., Song, J., Chen, Q., Kawamura, K., Wan, X., Kang, S., Wang, X., Laskin, A., and Cong, Z.:
889 Fluorescence characteristics of water-soluble organic carbon in atmospheric aerosol, Environmental Pollution, 268,
890 115906, 10.1016/j.envpol.2020.115906, 2021a.
891 Wu, G. M., Fu, P. Q., Ram, K., Song, J. Z., Chen, Q. C., Kawamura, K., Wan, X., Kang, S. C., Wang, X. P., Laskin,
892 A., and Cong, Z. Y.: Fluorescence characteristics of water-soluble organic carbon in atmospheric aerosol, Environ
893 Pollut, 268, ARTN 115906
894 10.1016/j.envpol.2020.115906, 2021b.
895 Xie, X., Chen, Y., Nie, D., Liu, Y., Liu, Y., Lei, R., Zhao, X., Li, H., and Ge, X.: Light-absorbing and fluorescent
896 properties of atmospheric brown carbon: A case study in Nanjing, China, Chemosphere, 251, 126350,
897 10.1016/j.chemosphere.2020.126350, 2020.
898 Yan, J., Wang, X., Gong, P., Wang, C., and Cong, Z.: Review of brown carbon aerosols: Recent progress and
899 perspectives, Sci Total Environ, 634, 1475-1485, 10.1016/j.scitotenv.2018.04.083, 2018.
900 Yu, H., Liang, H., Qu, F., Han, Z. S., Shao, S., Chang, H., and Li, G.: Impact of dataset diversity on accuracy and
901 sensitivity of parallel factor analysis model of dissolved organic matter fluorescence excitation-emission matrix,
902 Scientific Reports, 5, 10207, 10.1038/srep10207, 2015.
903 Yue, S., Zhu, J., Chen, S., Xie, Q., Li, W., Li, L., Ren, H., Sihui, S., Ping, L., Ma, H., Fan, Y., Cheng, B., Wu, L.,
904 Deng, J., Hu, W., Ren, L., Lianfang, W., Zhao, W., Tian, Y., and Fu, P.: Brown carbon from biomass burning
905 imposes strong circum-Arctic warming, One Earth, 5, 293-304, 10.1016/j.oneear.2022.02.006, 2022.
906 Yue, S. Y., Bikkina, S., Gao, M., Barrie, L., Kawamura, K., and Fu, P. Q.: Sources and Radiative Absorption of
907 Water-Soluble Brown Carbon in the High Arctic Atmosphere, Geophys Res Lett, 46, 14881-14891,
908 10.1029/2019gl085318, 2019.
909 Zhan, Y., Li, J., Tsona, N. T., Chen, B., Yan, C., George, C., and Du, L.: Seasonal variation of water-soluble brown
910 carbon in Qingdao, China: Impacts from marine and terrestrial emissions, Environmental Research, 212, 113144,
911 https://doi.org/10.1016/j.envres.2022.113144, 2022.

912   Zhang, Q., Jimenez, J. L., Canagaratna, M. R., Ulbrich, I. M., Ng, N. L., Worsnop, D. R., and Sun, Y.:
913   Understanding atmospheric organic aerosols via factor analysis of aerosol mass spectrometry: a review, Analytical
914   Chemistry and Bioanalytical Chemistry, 401, 3045-3067, 10.1007/s00216-011-5355-y, 2011.
915   Zhang, Q., Shen, Z., Zhang, T., Kong, S., Lei, Y., Wang, Q., Tao, J., Zhang, R., Wei, P., Wei, C., Cui, S., Cheng, T.,
916   Ho, S. S. H., Li, Z., Xu, H., and Cao, J.: Spatial distribution and sources of winter black carbon and brown carbon in
917   six Chinese megacities, Science of The Total Environment, 762, 143075,
918   https://doi.org/10.1016/j.scitotenv.2020.143075, 2021.
919   Zhong, M., and Jang, M.: Light absorption coefficient measurement of SOA using a UV–Visible spectrometer
920   connected with an integrating sphere, Atmospheric Environment, 45, 4263-4271, 10.1016/j.atmosenv.2011.04.082,
921   2011.
922   Zhu, C. S., Cao, J. J., Huang, R. J., Shen, Z. X., Wang, Q. Y., and Zhang, N. N.: Light absorption properties of
923   brown carbon over the southeastern Tibetan Plateau, Science of the Total Environment, 625, 246-251,
924   10.1016/j.scitotenv.2017.12.183, 2018.
925